DRAFT VERSION JANUARY 5, 2023
Typeset using LaTeX twocolumn style in AASTeX63

The *K2* & *TESS* Synergy II: Revisiting 26 systems in the *TESS* Primary Mission

ERICA THYGESEN [ID],[1] JESSICA A. RANSHAW [ID],[2] JOSEPH E. RODRIGUEZ [ID],[1] ANDREW VANDERBURG [ID],[3] SAMUEL N. QUINN [ID],[4]
JASON D. EASTMAN [ID],[4] ALLYSON BIERYLA [ID],[4] DAVID W. LATHAM [ID],[4] ROLAND K. VANDERSPEK,[3] JON M. JENKINS [ID],[5]
DOUGLAS A. CALDWELL [ID],[6,5] MMA IKWUT-UKWA [ID],[4] KNICOLE D. COLÓN [ID],[7] JESSIE DOTSON,[5] CHRISTINA HEDGES [ID],[5]
KAREN A. COLLINS [ID],[4] MICHAEL L. CALKINS [ID],[4] PERRY BERLIND,[4] GILBERT A. ESQUERDO [ID][4]

[1]Center for Data Intensive and Time Domain Astronomy, Department of Physics and Astronomy, Michigan State University, East Lansing, MI 48824, USA
[2]Indiana University Department of Astronomy, SW319, 727 E 3rd Street, Bloomington, IN 47405 USA
[3]Department of Physics and Kavli Institute for Astrophysics and Space Research, Massachusetts Institute of Technology, Cambridge, MA 02139, USA
[4]Center for Astrophysics | Harvard & Smithsonian, 60 Garden St, Cambridge, MA 02138, USA
[5]NASA Ames Research Center, Moffett Field, CA, 94035, USA
[6]SETI Institute, Mountain View, CA 94043, USA
[7]Exoplanets and Stellar Astrophysics Laboratory, Code 667, NASA Goddard Space Flight Center, Greenbelt, MD 20771, USA

ABSTRACT

The legacy of NASA's *K2* mission has provided hundreds of transiting exoplanets that can be revisited by new and future facilities for further characterization, with a particular focus on studying the atmospheres of these systems. However, the majority of *K2*-discovered exoplanets have typical uncertainties on future times of transit within the next decade of greater than four hours, making observations less practical for many upcoming facilities. Fortunately, NASA's Transiting Exoplanet Survey Satellite (*TESS*) mission is reobserving most of the sky, providing the opportunity to update the ephemerides for ∼300 *K2* systems. In the second paper of this series, we reanalyze 26 single-planet, *K2*-discovered systems that were observed in the *TESS* primary mission by globally fitting their *K2* and *TESS* lightcurves (including extended mission data where available), along with any archival radial velocity measurements. As a result of the faintness of the *K2* sample, 13 systems studied here do not have transits detectable by *TESS*. In those cases, we re-fit the *K2* lightcurve and provide updated system parameters. For the 23 systems with $M_* \gtrsim 0.6\,M_\odot$, we determine the host star parameters using a combination of *Gaia* parallaxes, Spectral Energy Distribution (SED) fits, and MESA Isochrones and Stellar Tracks (MIST) stellar evolution models. Given the expectation of future *TESS* extended missions, efforts like the *K2* & *TESS* Synergy project will ensure the accessibility of transiting planets for future characterization while leading to a self-consistent catalog of stellar and planetary parameters for future population efforts.

1. INTRODUCTION

The past two decades have been fruitful for exoplanet discovery, with over 5000 exoplanets confirmed to date[1]. While new discoveries are still being made, we are simultaneously venturing into an era of exploring known systems in further detail, with a variety of dedicated efforts for exoplanet characterization. Facilities that are operational or expected to be online in the next decade such as JWST (Gardner et al. 2006; Beichman et al. 2020), 39 m European Southern Observatory Extremely Large Telescope (ELT; Udry et al. 2014), Nancy Grace Roman Space Telescope (e.g. Carrión-González et al. 2021), Giant Magellan Telescope (Johns et al. 2012) and Atmospheric Remote-sensing Infrared Exoplanet Large-survey

(ARIEL; Tinetti et al. 2018, 2021) will provide key information about the atmospheres of exoplanets, and insight into their formation and evolutionary processes. However, these ongoing and future endeavors to reobserve known transiting exoplanets heavily rely on precisely knowing the transit time, which is challenged by the degradation of the ephemeris over time.

Most exoplanets and candidates found to date were originally discovered by the *Kepler* mission (Borucki et al. 2010). *Kepler* was launched in 2009 with the goal of understanding the demographics of transiting exoplanets. This mission was a success, having discovered ∼2700 confirmed planets with a further ∼2000 candidates[2], in addition to advancing our understanding of the host stars they orbit (e.g. Bastien et al. 2013; Berger et al. 2020a,b). However, by May of 2013

Corresponding author: Erica Thygesen
thygesen@msu.edu

[1] https://exoplanetarchive.ipac.caltech.edu/

[2] https://exoplanetarchive.ipac.caltech.edu/
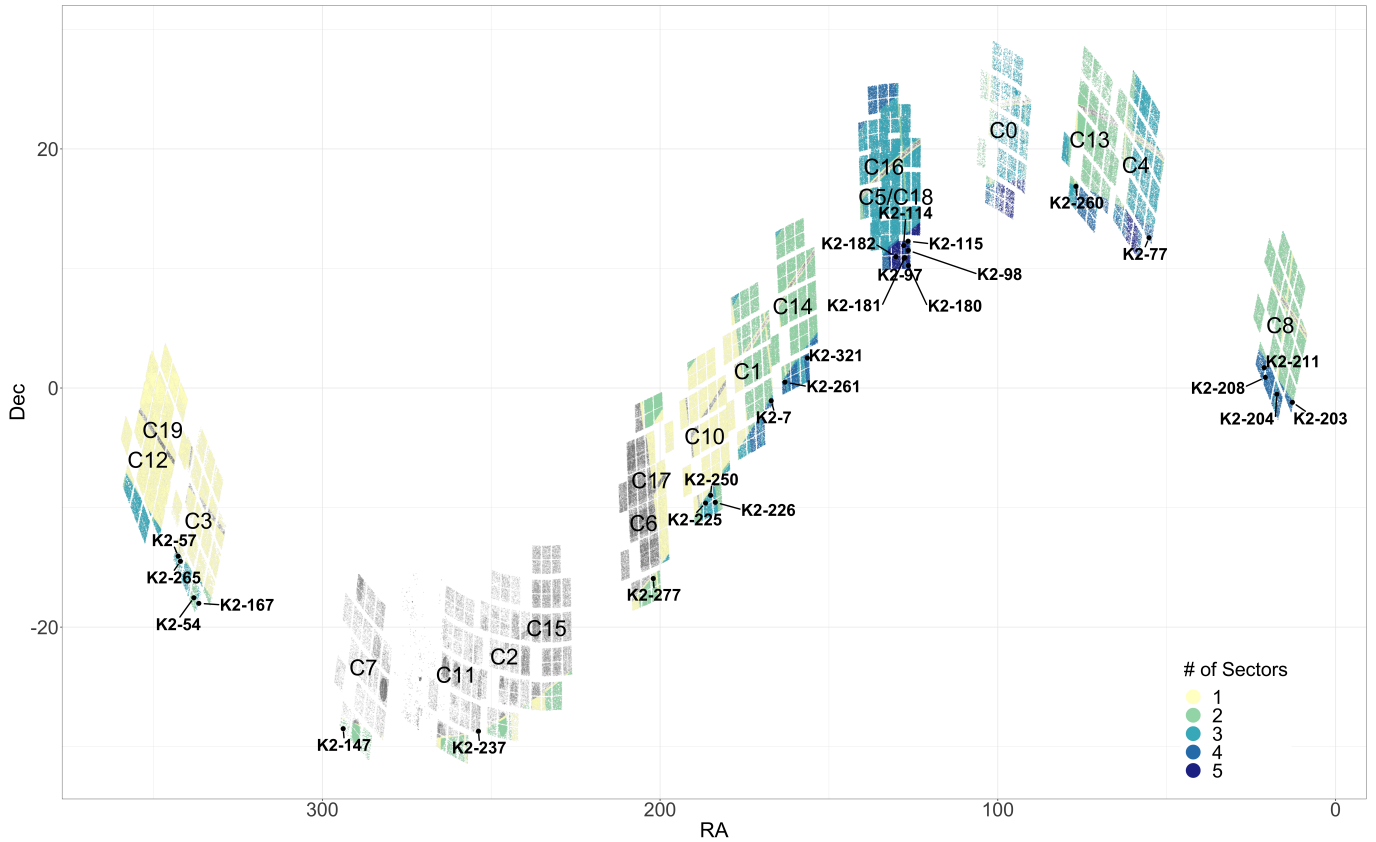
Figure 1. Overlap between *K2* campaigns and *TESS* sectors. The number of times each *K2* target was observed in *TESS* sectors is indicated by the color, with gray indicating no *TESS* overlap as of Sector 46. The systems analyzed in this study are labeled.

two of the four reaction wheels on the spacecraft had failed, severely limiting the pointing of *Kepler*, threatening to end the mission. A solution was conceived to point the spacecraft at the ecliptic to reduce torque from Solar radiation pressure, so that the remaining two reaction wheels, along with the thrusters, could maintain sufficient stability. This saw *Kepler* successfully reborn as the *K2* mission (Howell et al. 2014). While *Kepler* continuously pointed at one region of sky, the necessity of *K2* being aimed along the ecliptic opened up an opportunity to study different populations of stars. *K2* continued on the path of exoplanet discovery, with currently ∼500 confirmed planets and another ∼1000 candidates found by the time the spacecraft retired in 2018 when fuel for the thrusters ran out (Vanderburg et al. 2016; Zink et al. 2021; Kruse et al. 2019; Pope et al. 2016; Livingston et al. 2018b; Crossfield et al. 2016; Dattilo et al. 2019).

Unfortunately, many of the known planets discovered by the *K2* mission have not been reobserved since their discovery, leading to future transit time uncertainties of many hours (Ikwut-Ukwa et al. 2020). This has recently changed with the launch of NASA's *Transiting Exoplanet Survey Satellite* (*TESS*) mission in 2018 (Ricker et al. 2015), the successor to the *Kepler* and *K2* missions. The two-year primary mission of *TESS* aimed to observe more than 200,000 stars at

two-minute cadence across ∼75% of the sky. To date, *TESS* has found ∼280 confirmed planets and another ∼6100 candidates[3]. Even though *K2* targeted the ecliptic plane and the *TESS* primary mission only skimmed the edges of some *K2* fields, there are ∼30 systems that were observed by both (single- and multi-planet systems). This provides an opportunity to begin updating the ephemerides and parameters of *K2* systems that have been reobserved by *TESS*. The first extended mission of *TESS* began during 2020, and includes sectors dedicated to the ecliptic plane, providing more substantial overlap of a further ∼300 systems with the *K2* fields[4] (Figure 1). With *TESS* scheduled to reobserve nearly the entire sky during its extended missions, it will be a useful tool for refreshing the ephemerides of thousands of transiting exoplanets.

Currently, many known exoplanets do not have sufficiently accurate projected transit times to plan observations with future missions. Even *TESS* ephemerides will need to be updated as most *TESS* planets will have transit time uncertainties exceeding 30 minutes in the era of JWST (Dragomir et al.

---

[3] https://nexsci.caltech.edu/

[4] https://heasarc.gsfc.nasa.gov/docs/tess/the-tess-extended-mission.html

2020). With the wealth of data coming from ongoing surveys like *TESS* and the ability to follow up many planets with small aperture (<1 m) telescopes (Collins et al. 2018), many efforts have begun to keep the ephemerides of transiting planets from going stale, like the ExoClock Project (Kokori et al. 2021, 2022) for future ARIEL targets and the *K2* & *TESS* Synergy (Ikwut-Ukwa et al. 2020). Ephemeris refinement programs focused on citizen science (Zellem et al. 2019, 2020) and high-school students (e.g. ORBYTS; Edwards et al. 2019, 2020, 2021) also provide opportunities to actively engage the public while contributing to an essential aspect of future exoplanet characterization. These efforts will be key to making a large number of systems accessible for future facilities.

A continual renewal of ephemerides also presents an opportunity to create self-consistent catalogs of exoplanets and their parameters, which not only helps to plan for future missions, but also allows for appropriate population studies using data that have been uniformly prepared. While the vast amount of data available per system makes this a challenge, the advent of new exoplanet fitting suites to globally analyze large quantities of data, like `Juliet` (Espinoza et al. 2019), `EXOFASTv2` (Eastman et al. 2013; Eastman 2017; Eastman et al. 2019), `Allesfitter` (Günther & Daylan 2021) and `exoplanet` (Foreman-Mackey et al. 2021), has made it possible to individually model the available observations for a large sample of exoplanetary systems. These types of studies are necessary to uncover large-scale trends or mechanisms that may play important roles in planet formation and evolution. A renowned example is the radius valley of small planets (Fulton et al. 2017), which was achieved through more accurate and consistent handling of host star parameters for over 2000 planets from the California-*Kepler* Survey.

A case study for updating *K2* ephemerides and system parameters with new *TESS* data was presented in the first paper of this series (Ikwut-Ukwa et al. 2020), where four *K2*-discovered systems (K2-114, K2-167, K2-237 and K2-261) were reanalyzed by performing global fits using *K2* and *TESS* lightcurves. This resulted in the uncertainties for the transit times of all four planets being reduced from multiple hours to between 3-26 minutes (at a one sigma level) throughout the expected span of the JWST primary mission, showcasing the value of combining the *K2* and *TESS* data. We continue this work by reanalyzing a sample of 26 single-planet systems observed with *K2* and the primary *TESS* mission (including refitting the original four systems for consistency), while also making use of archival radial velocities, *Gaia* parallaxes and any currently available lightcurves from the *TESS* extended mission. We focus on previously-confirmed single-planet systems, but future papers in this series are expected to reanalyze all *K2* systems (including multi-planet systems) as part
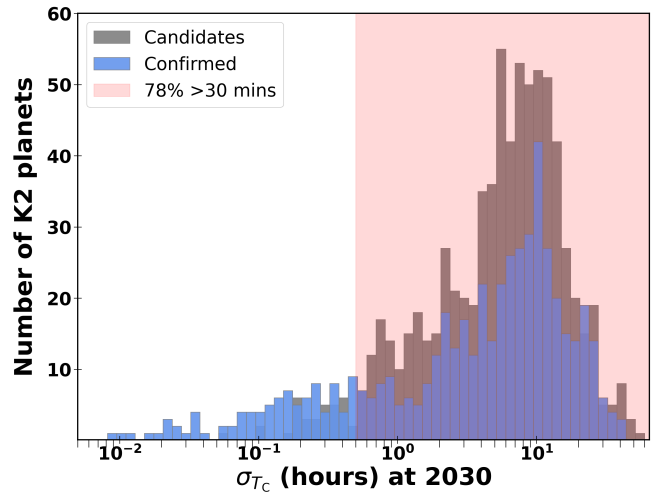
Figure 2. Uncertainty of the transit time (σ_{T_c}) for *K2* candidate and confirmed planets at the year 2030, based on the discovery ephemeris. The majority of planets have uncertainties greater than 30 minutes (indicated by the red region) in the era of JWST, making these challenging to reobserve. Values taken from the NASA Exoplanet Archive (NEA) default parameter sets.

of an ongoing *TESS* guest investigator program (G04205, PI Rodriguez). Updated transit times will be made available to the community throughout this series through the Exoplanet Follow-up Observing Program for TESS (ExoFOP)[5].

In §2 we describe how we obtained and prepared the data used in our global fits. §3 outlines how we ran the `EXOFASTv2` analysis, and §4 presents our results along with any peculiarities for specific systems. Our conclusions are summarized in §5.

2. OBSERVATIONS AND ARCHIVAL DATA

Given that most known *K2*-discovered exoplanet systems will have uncertainties larger than 30 minutes (see Figure 2), we take advantage of the high-quality data obtained with *K2* and *TESS*, simultaneously fitting the photometry and archival spectroscopy to update system parameters for 26 *K2* systems. Here we describe the techniques used to obtain and process *K2* and *TESS* lightcurves, as well as radial velocities from existing literature.

2.1. *K2 Photometry*

Each of these stars was observed by the *Kepler* spacecraft during its *K2* extended mission (Howell et al. 2014). During *K2*, the spacecraft's roll angle drifted significantly due to the failure of two reaction wheels, which introduced significant

---

[5] https://exofop.ipac.caltech.edu/tess/

systematic errors into its lightcurves[6]. Over the course of the mission, a number of different techniques and methods were developed to mitigate these errors (e.g. Aigrain et al. 2016; Barros et al. 2016; Luger et al. 2016; Lund et al. 2015; Pope et al. 2019). In this work, we used the methods of Vanderburg & Johnson (2014) and Vanderburg et al. (2016) to derive a rough systematics correction. In brief, these methods involve extracting raw lightcurves from a series of 20 different photometric apertures, correlating short timescale variations in the raw lightcurves with the spacecraft's roll angle (which changes rapidly due to K2's unstable pointing), and subtracting variability correlated with the spacecraft's roll angle. The process of correlating and subtracting variability correlated with the roll angle is performed iteratively until the only remaining variations in the lightcurve are unrelated to the spacecraft's roll. Finally, we select the aperture that produces the most precise lightcurve among the 20 originally extracted. Then, we refined the systematics correction by simultaneously fitting the transits for each planet along with the systematics correction and low-frequency stellar variability, prior to the final global fit. Most of the data we analyzed were collected in 30-minute long-cadence data, but when available, we analyzed 1-minute short-cadence exposures for better time sampling. For all systems, we only included out-of-transit data from one full transit duration before and after each transit. This is to optimize the balance between having enough data points to establish the baseline flux of the star and lengthening the runtime of the fits due to having more data.

2.2. *TESS Photometry*

While all 26 systems were initially observed by *TESS* in the primary mission, each was reobserved in at least one sector of the first extended mission. We therefore included *TESS* lightcurves from the primary and extended missions up to and including Sector 46 (as of February 1, 2022). This was the final sector dedicated to the ecliptic plane for the first extended mission. Future efforts in this series will analyze systems that were first observed by *TESS* during the first extended mission and beyond.

We used the Python package *Lightkurve* (Lightkurve Collaboration et al. 2018) to retrieve *TESS* lightcurves from the Mikulski Archive for Space Telescopes (MAST). Three systems within the footprint of the *TESS* primary mission (K2-42, K2-132/TOI 2643 and K2-267/TOI 2461) did not have corresponding retrievable lightcurves, which is likely due to being too close to the edge of the detector, so we excluded

these from the current analysis. For the *TESS* lightcurves, we used the Pre-search Data Conditioned Simple Aperture Photometry (PDCSAP) flux, which is the target flux within the optimal *TESS* aperture that has been corrected for systematics with the PDC module (Stumpe et al. 2012, 2014; Smith et al. 2012). Typically, observations for each sector are processed through the Science Processing Operations Center (SPOC) pipeline at the NASA Ames Research Center (Jenkins et al. 2016). The SPOC pipeline takes in the raw data and applies corrections for systematics, runs diagnostic tests and identifies transits, resulting in a calibrated lightcurve that can be used for analysis.

TESS science observations are taken at 20-second and 2-minute cadences (the former only becoming available from the first extended mission), while the Full Frame Images (FFIs) are created every 30 minutes during the primary mission, and every 10 minutes since the first extended mission. For our global analysis, (see §3) we used the shortest cadence available, preferentially using data processed through SPOC (Jenkins et al. 2016; Caldwell et al. 2020). The increased timing precision of short cadence observations is only valuable if there is a significant detection of the transit. For this reason, and since *TESS* is optimized for targets with brighter magnitudes than those of *K2*, we binned lightcurves observed at 20-second cadence to two minutes to increase signal-to-noise.

If a TESS-SPOC FFI lightcurve was not available for a particular sector, we extracted the lightcurve using a custom pipeline as described in Vanderburg et al. (2019). The pipeline uses a series of 20 apertures from which lightcurves are extracted and corrected for systematic errors from the spacecraft by decorrelating the flux with the mean and standard deviation of the quaternion time series. Dilution from neighbouring stars within the TIC is corrected for within each aperture, which takes into account the TESS pixel response function. The final aperture used for the lightcurve extraction is selected as the one that minimized the scatter in the photometry. Recent efforts have compared this custom pipeline with other FFI pipelines (Rodriguez et al. 2022), supporting our adoption of this pipeline. The list of available lightcurves (as of February 1, 2022) is shown in Table 1.

After retrieving the *TESS* lightcurves for our targets, we processed them further for our own analysis, assuming values for transit duration, time of conjunction (T_c) and period from the NASA Exoplanet Archive (NEA). To flatten the out-of-transit lightcurve for fitting, we used keplerspline[7], a spline-fitting routine to model and remove any variability from the star or remaining systematics (Vanderburg & Johnson 2014). Within keplerspline, the spacing between

---

[6] The two remaining reaction wheels onboard *K2* could control the position of the telescope's boresight, but the roll angle could only be controlled by occasional firing of the thrusters about every 6 hours as radiation pressure caused the telescope to slowly roll about its long axis.

[7] https://github.com/avanderburg/keplerspline

Table 1. Target list and data used in this analysis.

TIC ID	TOI	KID	EPIC ID	*K2* Campaign	*TESS* Sector (2 min)	(FFI)	RV instrument	*K2* Reference	*TESS* SNR
53210555	—	K2-7	201393098	C1	9, 36, 45, 46	—	—	1	5.62
12822545	—	K2-54[†]	205916793	C3	2, 42	—	—	2	1.76
146799150	—	K2-57	206026136	C3	2, 29	—	—	2	1.99
435339847	4544.01	K2-77	210363145	C4	5′, 42′, 43′, 44′	—	—	3	13.52
366568760	5121.01	K2-97	211351816	C5, C18	7′, 44′, 45′, 46′	—	LEVY[1] (6), HIRES[2] (18)	4	16.76
366410512	5101.01	K2-98	211391664	C5, C18	7, 34, 44, 45, 46	—	FIES[3] (4), HARPS[3] (4), HARPSN[3] (4)	5	20.93
366576758	514.01	K2-114	211418729	C5, C18	7, 44, 45, 46	—	HIRES[4] (5)	6	134.03
7020254	4316.01	K2-115	211442297	C5, C18	7, 34, 45, 46	—	HIRES[4] (7)	6	88.19
398275886	—	K2-147[†]	213715787	C7	27	13	—	7	2.91
69747919	1407.01	K2-167	205904628	C3	2, 28, 42,	—	—	3	13.82
366411016	5529.01	K2-180	211319617	C5, C18	34, 44, 45, 46	7*	HARPSN[5] (12)	8	12.03
366528389	—	K2-181	211355342	C5, C18	7, 44, 45, 46	—	—	3	5.74
366631954	5068.01	K2-182	211359660	C5, C18	34, 44, 45, 46	7	HIRES[6] (12)	9	32.39
333605244	—	K2-203	220170303	C8	30, 42, 43	3	—	3	3.17
248351386	—	K2-204	220186645	C8	30, 42, 43	3	—	3	5.44
399722652	—	K2-208	220225178	C8	30, 42, 43	3	—	3	4.76
399731211	—	K2-211	220256496	C8	30, 42, 43	3	—	7	2.90
98677125	—	K2-225	228734900	C10	36, 46	10	—	3	2.93
176938958	—	K2-226	228736155	C10	36, 46	10	—	3	3.82
16288184	1049.01	K2-237	229426032	C11	12, 39	—	CORALIE[7] (9), HARPS[7,8] (4,7), FIES[8] (9)	10	129.83
98591691	—	K2-250	228748826	C10	36, 46	10	—	11	3.79
293612446	2466.01	K2-260	246911830	C13	32, 43	5*	FIES[9] (18)	12	98.44
281731203	685.01	K2-261	201498078	C14	9, 35, 45, 46	—	FIES[9] (12), HARPS[9] (10), HARPSN[9] (8)	12	83.58
146364192	—	K2-265	206011496	C3	29, 42	2	HARPS[10] (138)	13	6.01
404421005	4628.01	K2-277	212357477	C6	10, 37′	—	—	4	8.75
277833995	5524.01	K2-321[†]	248480671	C14	8′, 45′, 46′	35′ (10min)	—	14	9.21

NOTES: *TESS* lightcurves taken at 20 second cadence were prioritised, and binned to two minutes. Where short cadence observations were not available, FFIs were used. *TESS* sectors in which transits had SNR≤7 and thus were too shallow to be recovered are colored red. We incorporated previous RV measurements that were taken from the previous studies listed here. The number in parentheses following the RV instrument indicates the number of measurements. *K2* references are previous analyses with which we compare our updated ephemerides in §4.

[†] The host stars in these systems were classed as low mass ($\lesssim 0.6\ M_\odot$), so we did not include the SEDs in the global fits. See §3 for details.

′ The full lightcurves for these were used to ensure the transit was able to be detected. All other lightcurves were sliced as discussed in §2.

* A custom pipeline was used to extract lightcurves for sectors without TESS-SPOC FFIs as discussed in §2.2.

References for RV measurements: [1]Grunblatt et al. (2016), [2]Grunblatt et al. (2018), [3]Barragán et al. (2016), [4]Shporer et al. (2017), [5]Korth et al. (2019), [6]Akana Murphy et al. (2021), [7]Soto et al. (2018), [8]Smith et al. (2019), [9]Johnson et al. (2018a), [10]Lam et al. (2018)

K2 references: 1 - Montet et al. (2015), 2 - Crossfield et al. (2016), 3 - Mayo et al. (2018), 4 - Livingston et al. (2018b), 5 - Barragán et al. (2016), 6 - Shporer et al. (2017), 7 - Adams et al. (2021), 8 - Korth et al. (2019), 9 - Akana Murphy et al. (2021), 10 - Soto et al. (2018), 11 - Livingston et al. (2018a), 12 - Johnson et al. (2018b), 13 - Lam et al. (2018), Castro González et al. (2020)

breaks in the spline to handle discontinuities is optimized by minimizing the Bayesian Information Criterion (BIC) for different break points (see Shallue & Vanderburg 2018 for further methodology). We applied a constant per-point error for the photometry, calculated as the median absolute deviation of the out-of-transit flattened lightcurve, although this error is optimized within our analysis since EXOFASTv2 fits a jitter term. If any lightcurve had large outliers or features that may influence our transit fit, we used only the data that had no bad quality flags within *Lightkurve* (this was only the case for K2-250 and K2-260). To reduce the individual runtime for each system, we excluded the out-of-transit baseline of the *TESS* lightcurves from the EXOFASTv2 fit other than one full transit duration before and after each transit (as with the *K2* lightcurves). However, for systems whose transits were not readily visually identified in the *TESS* data (K2-77, K2-97, K2-277 and K2-321; see Table 1), we included all out-

of-transit photometry to account for any large uncertainties in the time of transits during the *TESS* epochs.

2.3. *Archival Spectroscopy*

We identified spectroscopic observations from the literature for 10 of the 26 total targets (Figure 3; K2-97, K2-98, K2-114, K2-115, K2-180, K2-182, K2-237, K2-260, K2-261 and K2-265; Grunblatt et al. 2016, 2018; Barragán et al. 2016; Shporer et al. 2017; Korth et al. 2019; Akana Murphy et al. 2021; Soto et al. 2018; Smith et al. 2019; Johnson et al. 2018a; Lam et al. 2018). We selected data sets with four or more RV measurements to ensure more degrees of freedom in the global fit, thus avoiding overfitting the data. For this reason we do not include RVs for K2-77 (Gaidos et al. 2017) and K2-147 (Hirano et al. 2018). Table 1 lists the analyses from which we obtained each set of RVs that we incorporated in the global analysis (see §3). All but one of the systems
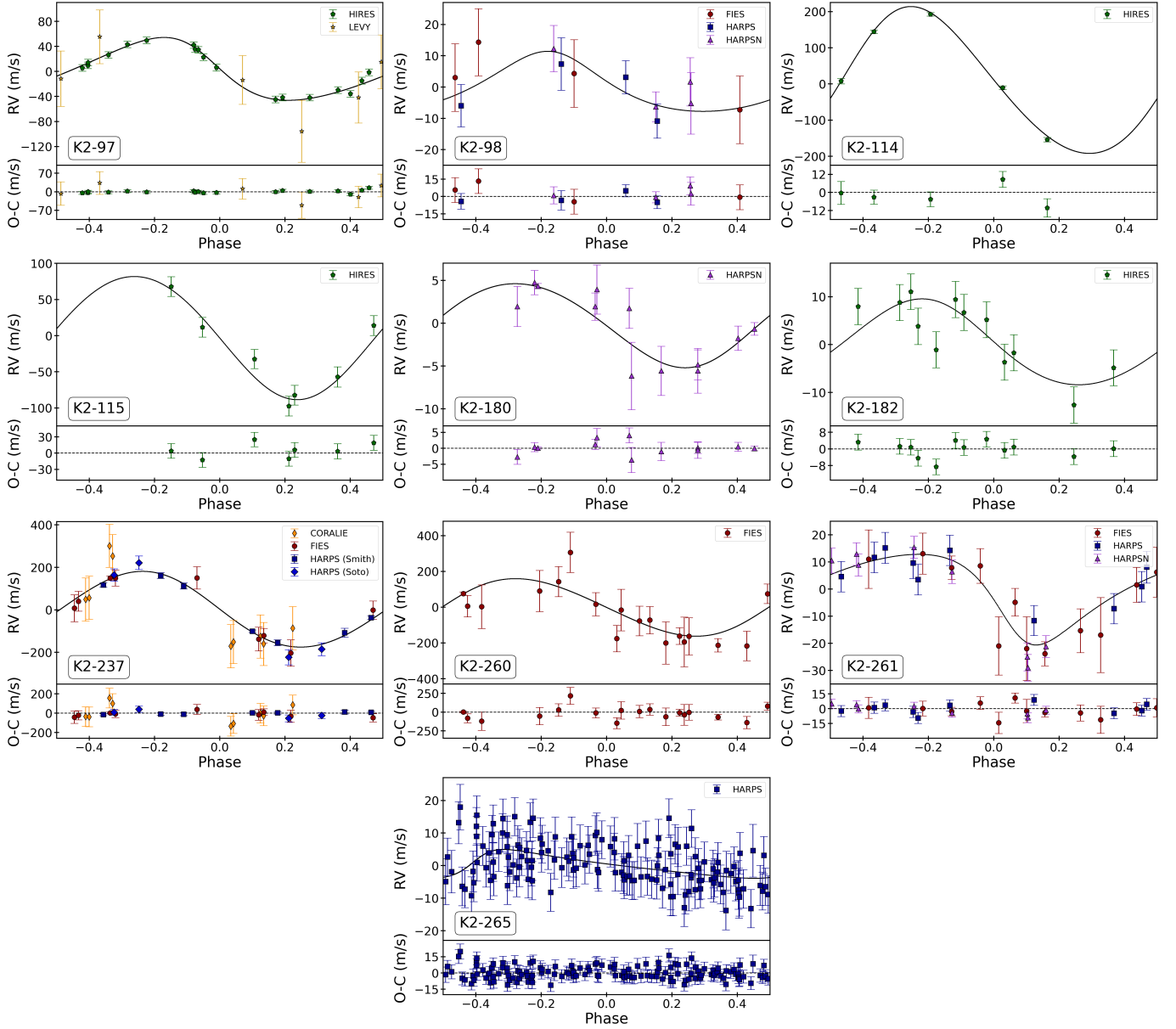
Figure 3. Radial velocities for the 10 systems with archival spectroscopic measurements. The best fit model from `EXOFASTv2` is shown in each subplot. Each set of RVs are phased using the best fit period and T_c determined in the fit, and the residuals are shown below each dataset. The references for each set of RVs are listed in Table 1.

that have RVs also have significant *TESS* transits (see §3), which is an outcome of spectroscopic measurements preferentially targeting brighter stars. The archival RVs were obtained from the following instruments: the Levy spectrometer on the 2.4m Automated Planet Finder at Lick Observatory, the High Resolution Echelle Spectrometer (HIRES) on the Keck-I Telescope (Vogt et al. 1994), the FIbre-fed Echelle Spectrograph (FIES) on the 2.56m Nordic Optical Telescope at Roque de los Muchachos Observatory Frandsen & Lindberg (1999), the High Accuracy Radial velocity Planet Searcher (HARPS) spectrograph on the 3.6m telescope at La Silla Observatory (Mayor et al. 2003), HARPS-N on the 3.58m Telescopio Nazionale Galileo at the Roque de los Muchachos Observatory (Cosentino et al. 2012), and the CORALIE spectrograph on the Swiss 1.2m Leonhard Euler Telescope at La Silla Observatory (Queloz et al. 2000).

If any determination for the host star's metallicity ([Fe/H]) was available, we included it as a prior in the fit to better constrain the host star parameters. For consistency, we used metallicity priors for most of the systems from spectra obtained using the Tillinghast Reflector Echelle Spectrograph (TRES; Fűrész 2008) on the 1.5m Tillinghast Reflector at the Fred L. Whipple Observatory (FLWO). Starting points were used for other stellar parameters where available, but no prior constraints were placed on any other values. We assumed the RV extraction and metallicity determination was done correctly in the discovery data. An RV jitter term is fit within the EXOFASTv2 analysis to ensure the uncertainties are properly estimated. In the cases of five or fewer RVs, we placed conservative uniform bounds on the variance of the jitter. The jitter variance for K2-114 and for the Soto et al. (2018) RVs for K2-237 were bounded to ±300 m/s, and for K2-98 the variance bounds were ±100 m/s for the FIES RVs, and ±4 m/s for HARPS and HARPS-N. For the HARPS RVs of K2-

265, we removed three clear outliers that were included in the discovery paper based on visual inspection[8].

3. GLOBAL FITS

To analyze the wealth of data for these 26 known *K2* exoplanet systems, we used EXOFASTv2 (Eastman et al. 2013, 2019; Eastman 2017) to perform global fits for our sample. EXOFASTv2 is an exoplanet fitting software package that uses MCMC sampling to simultaneously fit parameters for both the planets and host star. The *K2* and *TESS* photometric observations (Figures 4 and 5), along with any archival RVs (Figure 3), were jointly analyzed to obtain best-fit parameters for planets and host stars.

To characterize the host stars within each fit, we placed a uniform prior from 0 to an upper bound on line-of-sight extinction (A_v) from Schlegel et al. (1998) and Schlafly & Finkbeiner (2011), and Gaussian priors on metallicity ([Fe/H]) and parallax (using Gaia EDR3 and accounting for the small systematic offset reported; Gaia Collaboration et al. 2016, 2021; Lindegren et al. 2021). This also included the spectral energy distribution (SED) photometry as reported by Gaia DR2 (Gaia Collaboration et al. 2018), WISE (Cutri et al. 2012) and 2MASS (Cutri et al. 2003). These values are collated in Table 2, and all priors are listed in Tables 5-9. We excluded the WISE4 SED values for three systems that had this photometric measurement (K2-115, K2-225 and K2-237) due to the large uncertainties, and as there was a $\gtrsim 2\sigma$ discrepancy with the stellar model. Two other systems (K2-167 and K2-277) had WISE4 measurements that we used in the fits; these are consistent with the stellar models, but still have relatively large uncertainties. Within the EXOFASTv2 global fit, the MESA Isochrones and Stellar Tracks (MIST) stellar evolution models (Paxton et al. 2011, 2013, 2015; Choi et al. 2016; Dotter 2016) are used as the base isochrone to better constrain the host star's parameters.

Table 2. Literature Values.

Param.	Description	K2-7	K2-54	K2-57	K2-77	K2-97	K2-98	K2-114	K2-115
α_{J2016}	Right ascension (R.A.)	11:08:22.4996	22:32:12.9990	22:50:46.0386	03:40:54.8458	08:31:03.0808	08:25:57.1702	08:31:31.8984	08:26:12.8406
δ_{J2016}	Declination (Dec.)	-01:03:57.0898	-17:32:38.6338	-14:04:12.0152	+12:34:20.7938	+10:50:51.2025	+11:30:39.9313	+11:55:20.1168	+12:16:54.6527
G	Gaia DR2 G mag	13.057 ± 0.020	—	14.104 ± 0.020	11.920 ± 0.020	12.306 ± 0.020	12.040 ± 0.020	14.275 ± 0.020	13.200 ± 0.020
G_{Bp}	Gaia DR2 B_P mag	13.404 ± 0.020	—	14.781 ± 0.020	12.485 ± 0.020	12.895 ± 0.020	12.314 ± 0.020	14.806 ± 0.020	13.556 ± 0.020
G_{Rp}	Gaia DR2 R_P mag	12.552 ± 0.020	—	13.326 ± 0.020	11.236 ± 0.020	11.601 ± 0.020	11.616 ± 0.020	13.615 ± 0.020	12.689 ± 0.020
T	*TESS* mag	12.612 ± 0.008	—	13.383 ± 0.006	11.287 ± 0.006	11.652 ± 0.007	11.672 ± 0.008	13.667 ± 0.008	12.746 ± 0.006

Table 2 *continued*

3.1. *Stellar parameters*

---

[8] All parameters were within uncertainties when compared to an earlier fit including the outliers.

Table 2 *(continued)*

J	2MASS J mag	11.952 ± 0.022	—	12.350 ± 0.024	10.384 ± 0.020	10.694 ± 0.023	11.124 ± 0.022	12.835 ± 0.020	12.108 ± 0.021
H	2MASS H mag	11.628 ± 0.023	—	11.761 ± 0.022	9.910 ± 0.023	10.177 ± 0.023	10.905 ± 0.025	12.386 ± 0.030	11.760 ± 0.022
K_S	2MASS K_S mag	11.564 ± 0.021	—	11.645 ± 0.023	9.799 ± 0.020	10.035 ± 0.021	10.869 ± 0.028	12.304 ± 0.030	11.724 ± 0.020
WISE1	WISE1 mag	11.527 ± 0.030	—	11.586 ± 0.030	9.733 ± 0.030	9.990 ± 0.030	10.823 ± 0.030	12.230 ± 0.030	11.658 ± 0.030
WISE2	WISE2 mag	11.572 ± 0.030	—	11.639 ± 0.030	9.790 ± 0.030	10.090 ± 0.030	10.856 ± 0.030	12.326 ± 0.030	11.700 ± 0.030
WISE3	WISE3 mag	11.554 ± 0.233	—	11.506 ± 0.217	9.773 ± 0.054	10.026 ± 0.088	10.678 ± 0.108	—	11.723 ± 0.249
WISE4	WISE4 mag	—	—	—	—	—	—	—	—
μ_α	Gaia p.m. in R.A.	-4.657 ± 0.016	-5.018 ± 0.021	24.311 ± 0.022	22.425 ± 0.025	-1.239 ± 0.018	-16.165 ± 0.014	-13.062 ± 0.022	15.557 ± 0.018
μ_δ	Gaia p.m. in Dec.	-23.647 ± 0.012	-9.804 ± 0.018	-25.298 ± 0.019	-37.908 ± 0.015	-6.694 ± 0.013	-9.401 ± 0.010	-2.472 ± 0.016	-21.630 ± 0.012
π	Gaia parallax (mas)	1.451 ± 0.028	5.782 ± 0.033	3.818 ± 0.029	7.111 ± 0.043	1.241 ± 0.063	1.950 ± 0.042	2.130 ± 0.036	2.497 ± 0.025

Param.	K2-147	K2-167	K2-180	K2-181	K2-182	K2-203	K2-204	K2-208	K2-211
α_{J2016}	19:35:19.9267	22:26:18.2722	08:25:51.4492	08:30:12.9870	08:40:43.2088	00:51:05.6854	01:09:31.8015	01:23:06.9545	01:24:25.4797
δ_{J2016}	-28:29:54.5839	-18:00:42.0516	+10:14:47.6330	+10:54:36.5034	+10:58:58.6242	-01:11:45.1837	-00:31:03.9292	+00:53:20.4074	+01:42:17.6712
G	—	8.104 ± 0.020	12.404 ± 0.020	12.562 ± 0.020	11.720 ± 0.020	12.122 ± 0.020	12.889 ± 0.020	12.314 ± 0.020	12.933 ± 0.020
G_{Bp}	—	8.402 ± 0.020	12.817 ± 0.020	12.945 ± 0.020	12.190 ± 0.020	12.614 ± 0.020	13.223 ± 0.020	12.702 ± 0.020	13.399 ± 0.020
G_{Rp}	—	7.689 ± 0.020	11.839 ± 0.020	12.036 ± 0.020	11.122 ± 0.020	11.493 ± 0.020	12.408 ± 0.020	11.781 ± 0.020	12.333 ± 0.020
T	—	7.728 ± 0.006	11.896 ± 0.006	12.087 ± 0.006	11.170 ± 0.006	11.547 ± 0.006	12.461 ± 0.006	11.833 ± 0.006	12.383 ± 0.007
J	—	7.202 ± 0.021	11.146 ± 0.023	11.438 ± 0.022	10.408 ± 0.021	10.773 ± 0.024	11.839 ± 0.021	11.164 ± 0.026	11.624 ± 0.024
H	—	6.974 ± 0.038	10.747 ± 0.026	11.082 ± 0.021	9.994 ± 0.022	10.281 ± 0.026	11.569 ± 0.026	10.824 ± 0.022	11.205 ± 0.022
K_S	—	6.887 ± 0.034	10.677 ± 0.026	11.026 ± 0.021	9.913 ± 0.023	10.206 ± 0.023	11.478 ± 0.021	10.746 ± 0.020	11.104 ± 0.024
WISE1	—	6.810 ± 0.055	10.619 ± 0.030	10.999 ± 0.030	9.845 ± 0.030	10.145 ± 0.030	11.468 ± 0.030	10.697 ± 0.030	11.074 ± 0.030
WISE2	—	6.866 ± 0.030	10.667 ± 0.030	11.062 ± 0.030	9.917 ± 0.030	10.217 ± 0.030	11.507 ± 0.030	10.739 ± 0.030	11.128 ± 0.030
WISE3	—	6.906 ± 0.030	10.599 ± 0.099	11.041 ± 0.205	9.896 ± 0.054	10.100 ± 0.083	11.279 ± 0.173	10.645 ± 0.089	10.933 ± 0.093
WISE4	—	6.917 ± 0.100	—	—	—	—	—	—	—
μ_α	-31.399 ± 0.016	73.590 ± 0.028	97.243 ± 0.013	16.936 ± 0.014	-65.130 ± 0.029	-11.103 ± 0.021	-3.598 ± 0.026	-26.433 ± 0.019	48.694 ± 0.022
μ_δ	-147.502 ± 0.015	-114.502 ± 0.024	-89.214 ± 0.010	-33.182 ± 0.012	1.544 ± 0.022	0.450 ± 0.020	-30.522 ± 0.018	-39.656 ± 0.014	-10.262 ± 0.017
π	11.027 ± 0.033	12.457 ± 0.071	4.936 ± 0.041	2.805 ± 0.040	6.510 ± 0.052	5.937 ± 0.056	1.840 ± 0.052	3.859 ± 0.048	3.604 ± 0.055

Param.	K2-225	K2-226	K2-237	K2-250	K2-260	K2-261	K2-265	K2-277	K2-321	Ref.
α_{J2016}	12:26:09.8617	12:14:34.9587	16:55:04.5232	12:20:07.5686	05:07:28.1596	10:52:07.7541	22:48:07.5960	13:28:03.8821	10:25:37.3214	1
δ_{J2016}	-09:37:29.3675	-09:33:45.4617	-28:42:38.1039	-08:58:32.6688	+16:52:03.6985	+00:29:35.3793	-14:29:41.2159	-15:56:16.7278	+02:30:49.9241	1
G	11.520 ± 0.020	12.092 ± 0.020	11.467 ± 0.020	13.973 ± 0.020	12.467 ± 0.020	10.459 ± 0.020	10.928 ± 0.020	10.121 ± 0.020	—	2
G_{Bp}	11.929 ± 0.020	12.545 ± 0.020	11.776 ± 0.020	14.484 ± 0.020	12.798 ± 0.020	10.872 ± 0.020	11.337 ± 0.020	10.495 ± 0.020	—	2
G_{Rp}	10.984 ± 0.020	11.492 ± 0.020	11.013 ± 0.020	13.324 ± 0.020	11.974 ± 0.020	9.917 ± 0.020	10.364 ± 0.020	9.624 ± 0.020	—	2
T	11.028 ± 0.007	11.547 ± 0.006	11.066 ± 0.006	13.379 ± 0.006	12.036 ± 0.007	9.962 ± 0.007	10.422 ± 0.008	9.666 ± 0.006	—	3
J	10.362 ± 0.023	10.697 ± 0.023	10.508 ± 0.023	12.539 ± 0.026	11.400 ± 0.023	9.337 ± 0.030	9.726 ± 0.026	9.081 ± 0.034	—	4
H	10.046 ± 0.021	10.307 ± 0.023	10.268 ± 0.022	12.078 ± 0.022	11.189 ± 0.032	8.920 ± 0.042	9.312 ± 0.022	8.748 ± 0.071	—	4
K_S	9.954 ± 0.023	10.223 ± 0.023	10.217 ± 0.023	12.016 ± 0.024	11.093 ± 0.021	8.890 ± 0.022	9.259 ± 0.027	8.687 ± 0.024	—	4
WISE1	9.915 ± 0.030	10.166 ± 0.030	10.105 ± 0.030	11.878 ± 0.030	11.039 ± 0.030	8.828 ± 0.030	9.178 ± 0.030	8.630 ± 0.030	—	5
WISE2	9.978 ± 0.030	10.204 ± 0.030	10.129 ± 0.030	11.971 ± 0.030	11.036 ± 0.030	8.897 ± 0.030	9.213 ± 0.030	8.675 ± 0.030	—	5
WISE3	9.932 ± 0.057	10.118 ± 0.083	9.972 ± 0.077	11.534 ± 0.259	10.895 ± 0.129	8.819 ± 0.031	9.162 ± 0.040	8.649 ± 0.030	—	5
WISE4	—	—-	—	—	—	—	—	8.418 ± 0.261	—	5
μ_α	-38.138 ± 0.023	-22.324 ± 0.023	-8.568 ± 0.035	-50.359 ± 0.030	0.646 ± 0.018	-23.709 ± 0.020	30.138 ± 0.020	-98.828 ± 0.024	50.920 ± 0.025	1
μ_δ	-8.190 ± 0.017	2.109 ± 0.021	-5.625 ± 0.022	9.874 ± 0.018	-6.034 ± 0.013	-43.888 ± 0.017	-23.359 ± 0.016	-35.889 ± 0.016	-109.167 ± 0.022	1
π	2.796 ± 0.045	4.807 ± 0.074	3.298 ± 0.071	2.476 ± 0.036	1.498 ± 0.043	4.685 ± 0.043	7.189 ± 0.051	8.842 ± 0.062	13.009 ± 0.053	1

Notes. The uncertainties of the photometry have a systematic error floor applied. The SEDs were not used for K2-54, K2-147 and K2-321 (see §3).
Proper motions taken from the Gaia EDR3 archive and are in J2016. Parallaxes from Gaia EDR3 have a correction applied according to Lindegren et al. (2021).
Parallax for K2-277 is from Gaia DR2 and has been corrected according to Lindegren et al. (2018).
References: 1 - Gaia Collaboration et al. (2021), 2 - Gaia Collaboration et al. (2018), 3 - Stassun et al. (2018), 4 - Cutri et al. (2003), 5 - Cutri et al. (2012)

3.2. *Low-mass stars*

Stellar evolutionary models struggle to constrain low-mass stars ($\lesssim 0.6\ M_\odot$; Mann et al. 2015) and are thus unreliable.

For the three systems that fell into this category (K2-54, K2-147 and K2-321), we used the equations from Mann et al. (2015, 2019) that relate the apparent magnitude in the K_S band (M_{K_s}) to M_* and R_* to set a starting point with wide 5% Gaussian priors for these parameters. We excluded the SEDs from these fits and did not use the MIST models, fitting only the lightcurves (these systems did not have RV measurements). For this reason, we caution that the stellar parameters for these systems are unreliable. We also did not use the limb-darkening tables from Claret (2017) for the low-mass stars, as is the default in EXOFASTv2 for fitting the u_1 and u_2 coefficients, but rather placed starting points based on tables from Claret & Bloemen (2011) (Eastman et al. 2013) with a conservative Gaussian prior of 0.2 (Patel & Espinoza 2022).

3.3. *Contamination*

For systems with *TESS* contamination ratios specified in the *TESS* input catalog (TICv8, Stassun et al. 2018) and a clear transit detected in both *K2* and *TESS*, we fit for a dilution term[9] on the *TESS* photometry with a 10% Gaussian prior. This accounts for any nearby sources that may contribute flux to the target aperture that were unknown at the time the *TESS* Input Catalog was created. Although the *TESS* PDCSAP lightcurves are corrected for contamination, fitting the dilution allows an independent check on the contamination ratio correction performed by the SPOC pipeline. Fitting a dilution term for only the *TESS* photometry assumes the *K2* aperture has been correctly decontaminated or is comparatively uncontaminated, which is based on *K2* having a significantly smaller pixel scale than *TESS* (4" and 21" for *K2* and *TESS*, respectively). However, it is possible that there is still a level of contamination within the *K2* aperture that might be identified through high-resolution imaging. We checked the *K2* aperture for all of our targets to identify any major sources of contamination from the *Gaia* EDR3 catalog. We define contaminants as having flux ratios with the target star that are much larger than the uncertainties of the transit depth. To correct for the contaminating light, we followed the method from Rampalli et al. (2019) to account for the fraction of the flux within the aperture that belonged to our targets (F_{star}) as opposed to the contaminating stars based on the *Gaia* G-band fluxes. We found significant contamination for K2-54 ($F_{star} \approx 0.56$) and K2-237 ($F_{star} \approx 0.98$; the latter was originally discussed in Ikwut-Ukwa et al. 2020). Several other systems had potential faint contaminants, however, the global fit for the system with the next highest level of contamination (K2-250; $F_{star} \approx 0.98$) did not change within uncertainties before and after flux correction, so we did not

apply corrections to any systems other than K2-54 and K2-237.

3.4. *Global fits*

We ran a short preliminary fit for each system to identify any potential issues, e.g. particularly shallow transits, and then ran a final fit to convergence. For a fit to be accepted as converged, we adopted the default EXOFASTv2 criteria of $T_Z > 1000$, where T_Z is the number of independent draws, and a slightly loose Gelman-Rubin value of < 1.02 due to some transits being very shallow in *TESS*, resulting is long runtimes for the global fits. Within EXOFASTv2, we opted to reject all flat and negative transit models, which ensured a more reliable recovery of marginal transits (Eastman et al. 2019). We did not fit for transit timing variations, but plan to explore this in future papers.

Shallow transits clearly detected in *K2* were not always evident in the *TESS* lightcurves as the latter are necessarily noisier due to the smaller collecting area of the telescope (see §4.6 for discussion). For these systems we ran a *K2*-only fit to convergence and a short preliminary fit (Gelman-Rubin of ~ 1.1, $T_z \sim 100$). To assess whether it was advantageous to include the *TESS* lightcurves, we required certain criteria be met before running the *K2* and *TESS* fit to convergence. Firstly, we compared the improvement on uncertainties for parameters such as period and T_C, and projected these to the year 2030. If the uncertainties were notably smaller when including *TESS* data, we continued by visually inspecting the transits modelled by EXOFASTv2. For extremely marginal transits, we further binned the phased lightcurves to determine whether the transit was indeed visible. If the transit in *TESS* was still not obvious, we inspected the probability distribution functions (PDFs) output by EXOFASTv2 for clearly non-Gaussian distributions for key parameters, particularly period. If the period was not well-constrained (e.g. multimodal) even with the increased baseline of *TESS*, we excluded the *TESS* lightcurve from the fit. A multimodal period indicates that the MCMC identified different transit solutions based on the *TESS* data, implying that the *TESS* transits are not securely enough detected to update the ephemeris.

We ultimately excluded any *TESS* lightcurves where the transit has SNR $\lesssim 7$. As these are all previously confirmed planets, we adopted a less conservative SNR for bona fide transits in *TESS* compared to what is required for initial planet verification. This SNR threshold was chosen because the first system below this cut (K2-265, SNR = 6.0) had a multimodal posterior for period, and all other systems with lower SNR exhibited similar issues. Conversely, the system just above this threshold (K2-277, SNR = 8.1) has a broad but Gaussian period posterior, with no other systems above this SNR having unreliable PDFs.

---

[9] The starting point for dilution is calculated as D=C/(1+C).
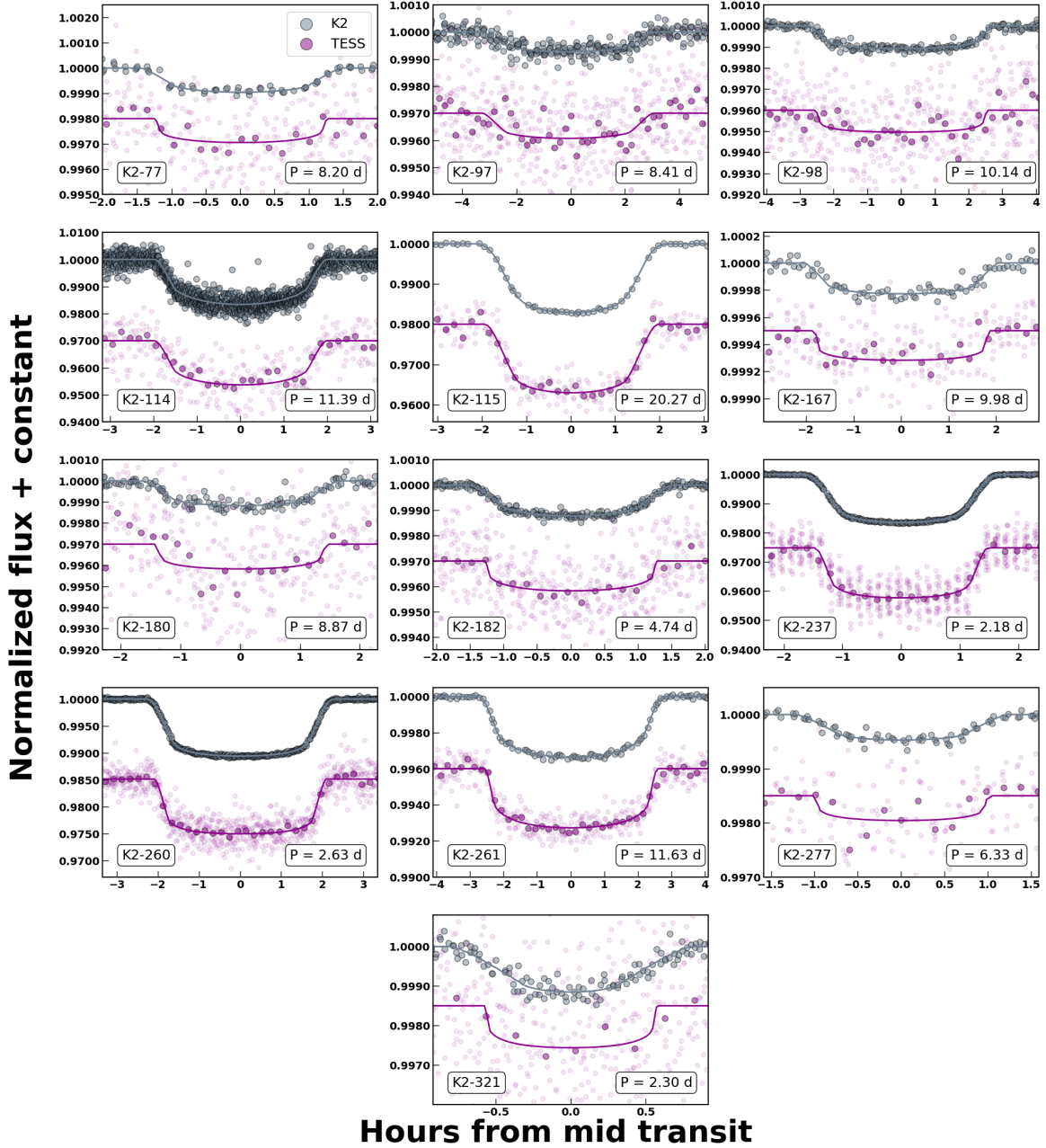
Figure 4. *K2* (gray) and *TESS* (purple) transits for all systems where *TESS* added significant value to the ephemeris projection. The phase-folded lightcurves include all data available across the *K2* campaigns and *TESS* sectors for each system, and have the best-fit model from `EXOFASTv2` overlaid (see Eastman et al. 2013, 2019; Eastman 2017 for how this is calculated). The system *K2* identifier and orbital period of the planet are displayed in each subplot. The *TESS* lightcurves are shown binned to 12 minutes, and the *K2* lightcurves are unbinned. For K2-237, the discreteness of the points is likely due to the period being an integer multiple of the exposure time.

Using this threshold, 13 of the 26 systems did not have recoverable *TESS* transits, so these were globally fit using only their *K2* lightcurves (Figure 5). While these systems will not have as significant improvement on their ephemerides, we still provide the updated parameters to include them in our final catalog of self-consistent parameters.

4. RESULTS AND DISCUSSION

We updated the system parameters for 26 single-planet systems discovered by *K2* and reobserved by *TESS*, four of which were part of the pilot study for the *K2* & *TESS* Synergy (K2-114, K2-167, K2-237 and K2-261; Ikwut-Ukwa et al. 2020). Tables 5-12 contain parameters from the global fits. Here we address any points of interest for individual systems and for the sample as a whole.
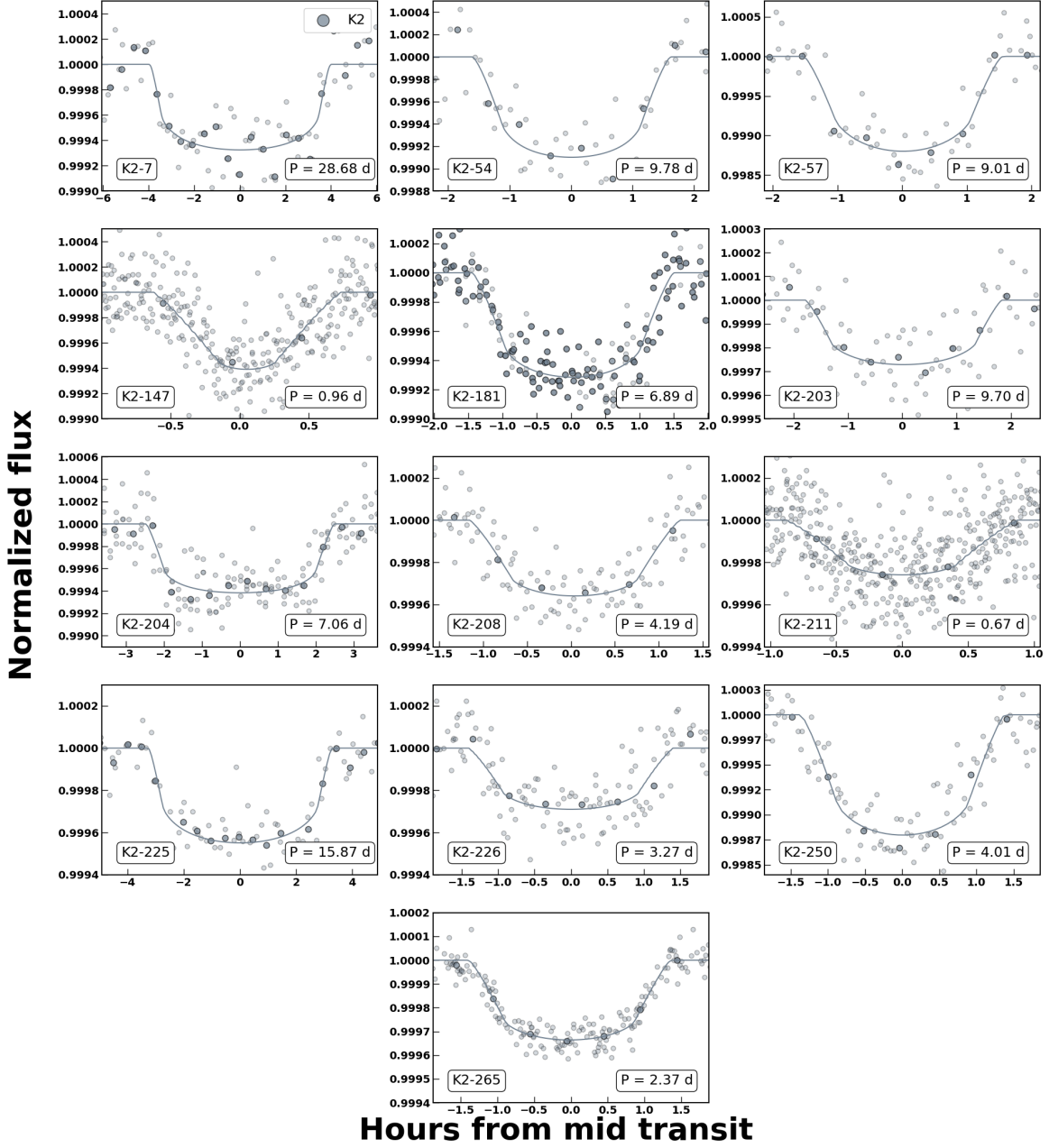
Figure 5. *K2* transits for systems that were not recoverable in *TESS* lightcurves. The darker points are binned to 30 minutes, and the `EXOFASTv2` best-fit model is shown.

.

4.1. *Ephemeris improvement*

As addressed in §1, a major incentive for refitting all *K2* and *TESS* systems is to update their ephemerides to provide the community with accurate transit times for observing with existing and upcoming facilities. Figures 6 and 7 show the projected transit timing uncertainties for our sample extrapolated to 2035, with markers indicating the expected launches for ongoing and future missions. The uncertainties on the

transit times are calculated by standard error propagation,

$$\sigma_{t_{\text{trans}}} = \sqrt{\sigma_{T_0}^2 + (n_{\text{trans}} \times \sigma_P)^2} \qquad (1)$$

where $\sigma_{t_{\text{trans}}}$ is the uncertainty on future transit time, σ_{T_0} is the uncertainty on the fitted optimal time of conjunction, n_{trans} is the number of transits that occurred between timestamps and σ_P is uncertainty on the period. For the future transit times using the results of the `EXOFASTv2` global fits, we used the optimal time of conjunction in order to minimize the covariance between T_C and P. However, T_0 is not generally avail-

able for the *K2* discovery parameters, so for the projected uncertainties on transit times for the original *K2* values we used T_C.

As expected, systems for which we excluded the *TESS* data due to shallow transits were not improved on the same scale as those with significant *TESS* transits. For the *K2* and *TESS* systems, the updated global fits were able to reduce most uncertainties from hours to minutes within the scope of some of the major facilities in the near future (Figure 6). For the 13 systems with detected *TESS* transits, the average 3σ uncertainty on the future transit time by the year 2030 was reduced from 26.7 to 0.35 hours (Table 3).

Systems for which we only included the *K2* lightcurves had significantly less improvement on the precision of predicted transit times. However, the ephemeris for K2-181 was considerably refined due to the addition of data from *K2* Campaign 18, which was not included in any previous analysis of this system. Excluding K2-181, there was a slight reduction of the average 3σ uncertainty from 43.2 to 35.6 hours (Table 4). The small improvement for some systems is likely due to using optimized *K2* lightcurves obtained from the pipeline described in §2.1, in conjunction with our fits including both the planet and the host star.

For systems with RV measurements, our ephemeris comparison uses uncertainties taken from previous analyses that included the RVs along with the *K2* data. The uncertainties for systems without RVs are taken from the most recent study that included lightcurves from *K2*. There are a handful of exceptions to this rule: for K2-77 we use the values from Mayo et al. (2018) as Gaidos et al. (2017) only has three RV measurements which is insufficient for our EXOFASTv2 fits; for K2-97, we use the values from Livingston et al. (2018b) as no T_c was presented in the analysis by Grunblatt et al. (2018) that included RVs; for K2-237 we use the less precise values from Soto et al. (2018) which are consistent with our results, rather than from Smith et al. (2019) which have a $\sim 4\sigma$ discrepancy with our findings (this was also found in Paper I; Ikwut-Ukwa et al. 2020).

As mentioned in §3.4, half of our sample did not have transits deep enough to be recovered by *TESS*. This presents a challenge for updating the transit times for these systems. If these systems are observed in future *TESS* sectors, it is possible that the SNR will increase sufficiently to include in a global fit. We will continue to monitor these and will include them in future releases, if this is the case.

4.1.1. *K2-167*

We note the use of an errant stellar metallicity prior used in the pilot study, where 0.45 instead of -0.45 (as reported by Mayo et al. 2018) was used as the Gaussian center. While this may have affected the solutions of stellar and plane-

Table 3. Ephemerides as of discovery compared to our updated values for systems with *K2* and *TESS* transits, with the 3σ uncertainty on future transit time by the year 2030.

	P (days)	T_c (BJD)	$3\sigma_{2030}$	TSM
K2-77				
Discovery	$8.199814^{+0.000364}_{-0.000367}$	$2457070.806480^{+0.001511}_{-0.001449}$	17.4 hr	
Updated	$8.2000844^{+0.0000086}_{-0.0000073}$	$2457316.80766^{+0.00099}_{-0.00096}$	22 min	27.3
K2-97				
Discovery	$8.406726^{+0.001863}_{-0.001827}$	$2457142.04977^{+0.00888}_{-0.00854}$	84.8 hr	
Updated	8.407115 ± 0.000023	$2457722.1447^{+0.0027}_{-0.0026}$	58 min	—
K2-98				
Discovery	10.13675 ± 0.00033	2457145.9807 ± 0.0012	12.6 hr	
Updated	$10.1367349^{+0.0000094}_{-0.0000092}$	$2457662.95321^{+0.00077}_{-0.00074}$	19 min	13.5
K2-114				
Discovery	$11.39109^{+0.00018}_{-0.00017}$	$2457174.49729 \pm 0.00033$	5.9 hr	
Updated	$11.3909310^{+0.0000031}_{-0.0000032}$	$2457687.08869 \pm 0.00016$	6 min	—
K2-115				
Discovery	$20.273034^{+0.000036}_{-0.000037}$	$2457157.15701 \pm 0.00025$	42 min	
Updated	20.2729914 ± 0.0000050	$2457522.07014 \pm 0.00017$	5 min	—
K2-167				
Discovery	$9.977481^{+0.001039}_{-0.001007}$	$2456979.936780^{+0.002518}_{-0.002443}$	40.8 hr	
Updated	$9.978541^{+0.000023}_{-0.000019}$	$2457299.2465^{0.0022}_{0.0023}$	48 min	46.1
K2-180				
Discovery	8.8665 ± 0.0003	2457143.390 ± 0.002	13.0 hr	
Updated	$8.865663^{0.000011}_{0.000010}$	$22457489.15656^{+0.00078}_{-0.00076}$	26 min	15.1
K2-182				
Discovery	4.7369683 ± 0.0000023	$2457719.11517 \pm 0.00028$	10 min	
Updated	4.7369696 ± 0.0000017	$2457652.79755^{+0.00027}_{-0.00028}$	8 min	15.4
K2-237				
Discovery	2.18056 ± 0.00002	2457684.8101 ± 0.0001	3.2 hr	
Updated	$2.18053332 \pm 0.00000054$	$2457706.61618^{+0.00003}_{-0.00003}$	5 min	—
K2-260				
Discovery	2.6266657 ± 0.0000018	$2457820.738135 \pm 0.00009$	14 min	
Updated	$2.62669762 \pm 0.00000066$	$2457894.284876^{+0.000060}_{-0.000059}$	5 min	—
K2-261				
Discovery	11.63344 ± 0.00012	$2457906.84084^{+0.00054}_{-0.00067}$	3.4 hr	
Updated	11.6334681 ± 0.0000044	$2458151.14394^{+0.00026}_{-0.00030}$	7 min	85.5
K2-277				
Discovery	$6.326763^{+0.000355}_{-0.000361}$	$2457221.22958^{+0.00221}_{-0.00217}$	21.5 hr	
Updated	$6.326768^{+0.000015}_{-0.000012}$	2457303.4771 ± 0.0010	48 min	35.6
K2-321				
Discovery	2.298 ± 0.001	2457909.17	144.0 hr	
Updated	$2.2979749^{+0.0000017}_{-0.0000019}$	$2458141.26759^{+0.00064}_{-0.00068}$	15 min	—

NOTES: The discovery values are taken from the *K2* references listed in Table 1. The T_C for the updated values is T_0 as determined by our global fits.
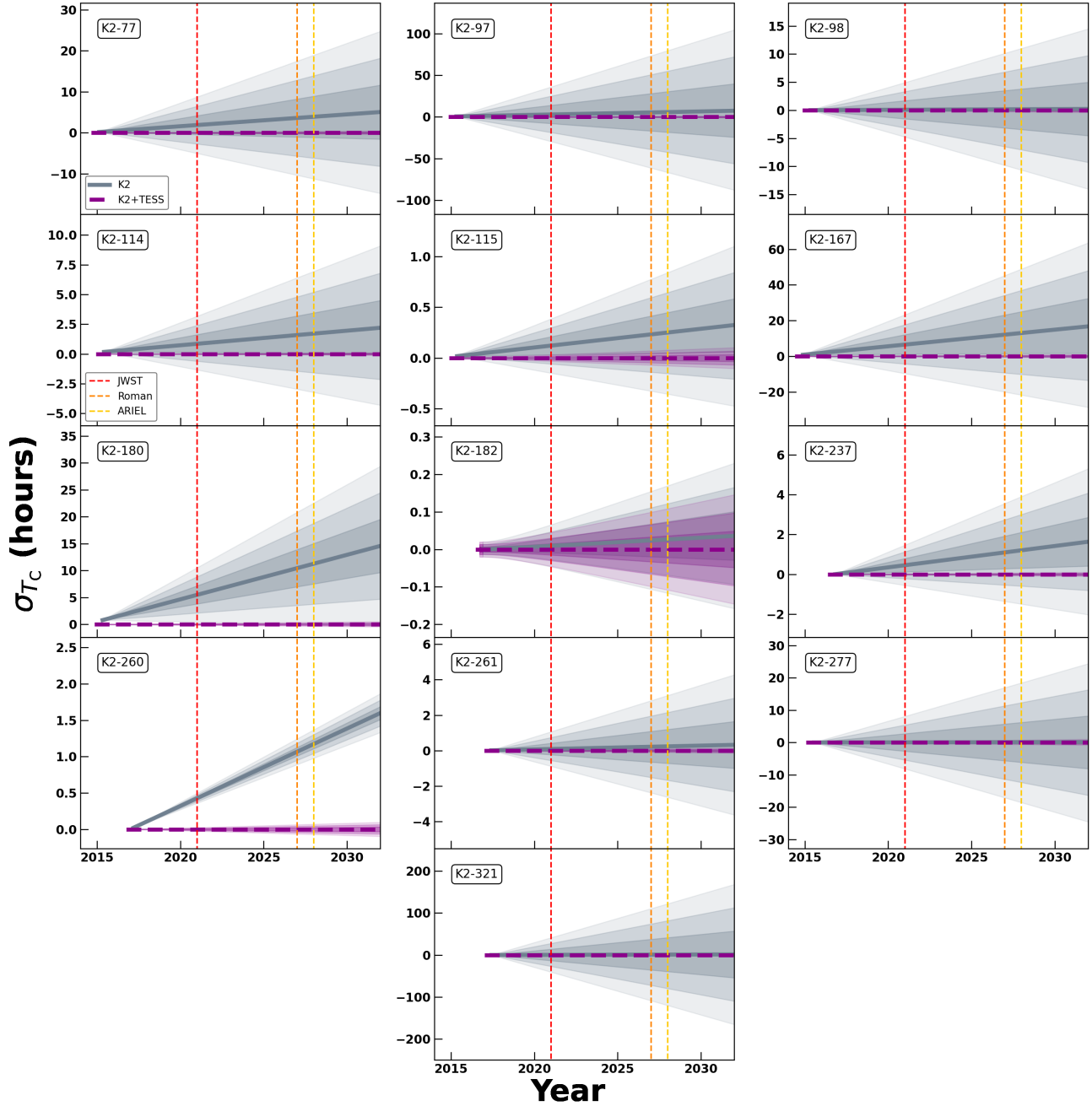
Figure 6. Projected uncertainties for transit times (σ_{T_c}) for systems with transits detected in both *K2* and *TESS*. The shaded regions represent the 1, 2 and 3 σ uncertainties, where gray is the uncertainty from the *K2* ephemerides listed in Table 1 and purple is our updated version using `EXOFASTv2`. The vertical dashed lines show the expected or actual launch years for missions for which these systems would be prospective targets (*JWST*: red, *NGRST*: orange, *ARIEL*: yellow). Note the y-axis scale is different in each subplot.

tary parameters, it would not have significantly altered the ephemeris.

4.1.2. *K2-260*

There is a clear discrepancy between the previously published ephemeris and our updated version (see Figure 6), well beyond a 3σ level. To test whether this was an artifact of our global fit, we ran a fit using only the *K2* lightcurves and com-

pared the results to the original and *K2* and *TESS* fits. Our *K2*-only fit was consistent with our *K2* and *TESS* ephemeris, and still in disagreement with the original results, suggesting that our updated fit provides the optimal ephemeris. It is possible that the original lightcurves introduced systematics in the discovery analysis, or the inclusion of additional follow-up data affected the ephemeris, but this is not clear. In any case, the consistency between our *K2*-only and *K2* and *TESS*
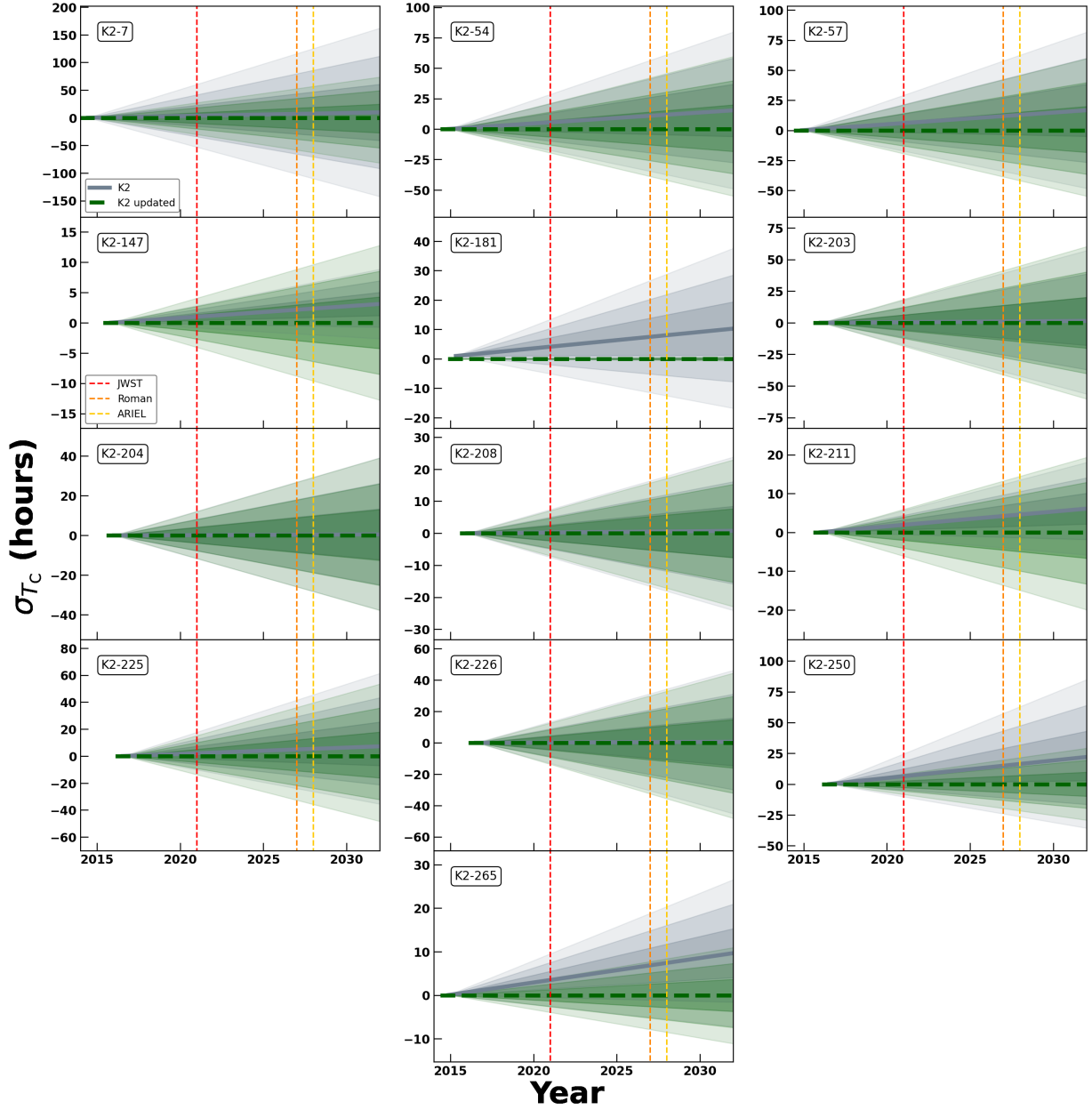
Figure 7. Same as Figure 6 but for systems with transits only detectable in the *K2* lightcurves. The shaded regions represent the 1, 2 and 3 σ uncertainties, where gray is the uncertainty from the *K2* ephemerides listed in Table 1 and green is our updated version using `EXOFASTv2`. The vertical dashed lines show the expected or actual launch years for missions for which these systems would be prospective targets (*JWST*: red, *NGRST*: orange, *ARIEL*: yellow). The ephemeris for K2-181 is significantly improved due to the inclusion of data from *K2* Campaign 18.

ephemerides (and no other system showing similar issues) gives us confidence in our results.

4.1.3. *K2-261*

As discussed in the pilot study (Ikwut-Ukwa et al. 2020), the PDFs for some stellar parameters (particularly age and mass) of K2-261 exhibit distinct bimodality that is likely due to the star being at a main sequence transition point (and not associated with the poor fits of shallow transits discussed in §3.4), causing difficulties with fitting the MIST isochrones

to the data to constrain age. We followed the same procedure from Ikwut-Ukwa et al. (2020), splitting the posterior at the minimum probability for M_* between the two Gaussian peaks (at M_*=1.19 $M_\odot$; see Figure 5 of Ikwut-Ukwa et al. 2020) and extracting two separate solutions for each peak. We list both solutions in Table 9, however, we use the low-mass solution for all figures as this has the higher probability. The different stellar mass solutions do not affect the ephemeris projection for this planet.

Table 4. Ephemerides as of discovery compared to our updated values for systems with only *K2* transits, with the 3σ uncertainty on future transit time by the year 2030.

	P (days)	T_c (BJD)	$3\sigma_{2030}$	TSM
K2-7				
Discovery	28.67992 ± 0.00947	2456824.6155 ± 0.0149	135.0 hr	
Updated	$28.6781^{+0.0046}_{-0.0051}$	$2456853.2946^{+0.0046}_{-0.0042}$	68.8 hr	5.9
K2-54				
Discovery	9.7843 ± 0.0014	2456982.9360 ± 0.0053	56.8 hr	
Updated	$9.7833^{+0.0013}_{-0.0012}$	2457002.5042 ± 0.0029	50.6 hr	—
K2-57				
Discovery	9.0063 ± 0.0013	2456984.3360 ± 0.0048	57.3 hr	
Updated	$9.0073^{+0.0012}_{-0.0011}$	2457011.3568 ± 0.0023	50.4 hr	10.8
K2-147				
Discovery	0.961918 ± 0.000013	$2457327.91683^{+0.00089}_{-0.00100}$	5.0 hr	
Updated	0.961939 ± 0.000029	$2457343.30907^{+0.00100}_{-0.00099}$	11.2 hr	—
K2-181				
Discovery	$6.894252^{+0.000430}_{-0.000426}$	$2457143.793550^{+0.002559}_{-0.002528}$	23.9 hr	
Updated	6.893813 ± 0.000011	2457778.0262 ± 0.0012	0.5 hr	14.6
K2-203				
Discovery	$9.695101^{+0.001285}_{-0.001334}$	$2457396.638780^{+0.005765}_{-0.005844}$	49.7 hr	
Updated	9.6952 ± 0.0014	$2457435.4189^{+0.0037}_{-0.0036}$	52.7 hr	1.3
K2-204				
Discovery	$7.055784^{+0.000650}_{-0.000641}$	$2457396.50862^{+0.00372}_{-0.00376}$	33.6 hr	
Updated	$7.05576^{+0.00066}_{-0.00064}$	2457431.7872 ± 0.0022	33.6 hr	11.1
K2-208				
Discovery	$4.190948^{0.000230}_{-0.000248}$	$2457396.51164^{+0.00248}_{-0.00235}$	21.0 hr	
Updated	4.19097 ± 0.00023	2457430.0390 ± 0.0016	20.0 hr	12.9
K2-211				
Discovery	0.669532 ± 0.000019	$2457395.82322 \pm 0.00160$	10.4 hr	
Updated	$0.669561^{+0.000031}_{-0.000032}$	2457432.6479 ± 0.0013	17.2 hr	2.1
K2-225				
Discovery	$15.871455^{+0.002113}_{-0.001670}$	$2457587.368230^{+0.004034}_{-0.004872}$	42.2 hr	
Updated	$15.8723^{+0.0021}_{-0.0019}$	$2457619.1111^{+0.0031}_{-0.0030}$	44.3 hr	11.1
K2-226				
Discovery	$3.271106^{+0.000367}_{-0.000369}$	$2457584.026130^{+0.004436}_{-0.004366}$	39.8 hr	
Updated	$3.27109^{+0.00036}_{-0.00039}$	2457620.0082 ± 0.0020	40.3 hr	14.6
K2-250				
Discovery	$4.01457^{+0.00062}_{-0.00057}$	$2457584.1212^{+0.0061}_{-0.0066}$	52.5 hr	
Updated	4.01392 ± 0.00029	2457620.2535 ± 0.0015	25.4 hr	13.8
K2-265				
Discovery	2.369172 ± 0.000089	2456981.6431 ± 0.0016	14.9 hr	
Updated	$2.369020^{+0.000058}_{-0.000059}$	$2457017.18078^{+0.00055}_{-0.00054}$	9.8 hr	15.7

NOTES: The discovery values are taken from the *K2* references listed in Table 1. The T_C for the updated values is T_0 as determined by our global fits.

4.1.4. *Comparison to pilot study*

The ephemerides were slightly improved for the four systems from the pilot study, the most significant being K2-167 (1.1 hours to 48 minutes) and K2-261 (30 minutes to 7 minutes). We did not expect to see major improvement because the baseline of new *TESS* sectors is relatively short compared to that of *K2* and the *TESS* primary mission.

4.2. *TSM*

We calculated the transmission spectroscopy metric (TSM; Kempton et al. 2018) for the planets in this sample to gauge the value of atmospheric follow-up (Tables 3 & 4; Figure 8). As the TSM is dependent on stellar parameters, we excluded the three systems for which we did not fit the host star (K2-54, K2-147, K2-321; see §3). The TSM is only valid for planets with $R_p < 10\,R_\oplus$, which removes a further five planets from this calculation (K2-97, K2-114, K2-115, K2-237 and K2-260). Only one system, K2-261, has a TSM above the threshold suggested by Kempton et al. (2018), and falls between the second and third quartile for the corresponding mass bin (see Table 1 of Kempton et al. 2018.) Future work in this project to update ephemerides will prioritize planets with high TSMs relative to the entire *K2* catalog.

4.3. *The sample*

While the systems in this analysis span a broad range of stellar temperatures and planet masses, most planets have orbital periods $\lesssim 10$ days and radii $\lesssim 5\,R_\oplus$ (Figures 8 and 9). Planet masses range from $2.6 \sim 639\,M_\oplus$ and host stars include M dwarfs to F-type spectral classifications. This demonstrates the diversity of the original *K2* sample as largely community-selected targets. Figure 9 shows how this sample compares to other known exoplanets.

4.4. *TTVs*

We did not fit for transit timing variations (TTVs) in this study. We would expect these to manifest as a significant change in ephemeris over time, whereas all of the systems studied here have updated ephemerides consistent to within 3σ of the original *K2* ephemeris (except K2-260; see §4.1.2). Therefore, any TTVs that may be present are currently too small to detect for these systems. Differences in the ephemerides on the $1 \sim 3\sigma$ level are likely due to the addition of the *TESS* lightcurves.

4.5. *Candidate planets*

We note that a couple of the systems in our analysis have additional candidate planets (K2-203 and K2-211). However, we ignore these for the purpose of updating ephemerides of

known exoplanets that are more likely future targets for missions such as JWST, but plan to revisit these in a future paper addressing multi-planet systems.

4.6. *K2 vs. TESS*

It is not surprising that relatively shallow *K2* transits were not detected by *TESS*. *Kepler* and *TESS* were designed to observe different stellar demographics, resulting in different photometric capabilities. *Kepler* was built with the intent to explore the number of near-Earth-sized planets close to their respective habitable zones around distant stars with apparent magnitudes $\lesssim 16$. The original *Kepler* mission could reach a precision of ~ 20 parts per million (ppm), which was generally the same for the *K2* mission (Vanderburg & Johnson 2014; Vanderburg et al. 2016).

On the other hand, *TESS* is focused on nearby, brighter stars with magnitude $\lesssim 12$. The precision of *TESS* has a floor at ~ 20 ppm at 1 hour for the brightest stars with $T_{mag} < 4$, but is more realistically $\gtrsim 100$ ppm for the majority of stars. Due to the all-sky nature of the *TESS* missions, observing sectors last on average 27 days for efficient sky coverage. *K2* campaigns were around 80 days in duration, meaning the same targets may have ~ 3 times as many transits observed by *K2*.

While *TESS* may not be able to recover all *K2* systems, the ones it can detect will have vastly improved ephemerides as demonstrated in Figure 6. Our analysis indicates *TESS* transits with SNR $\gtrsim 7$ are recoverable, and while this places a limit on the scope of this reanalysis, we can potentially gain access for reobservation of at least half of known *K2* planets. It is possible that future *TESS* missions that reobserve the planets with currently marginal transits (SNR $\sim 5-6$) will increase the SNR enough for a significant detection. However, for transits with SNR $\lesssim 5$, it is unlikely that more *TESS* observations will result in recoverable transits.

4.7. *Future work*

With several major facilities able to characterize exoplanets in extensive detail planned to come online within the next decade, not having accurate and precise transit times is a relevant issue. The *K2 & TESS* Synergy aims to solve the problem of degrading ephemerides for all *K2* systems reobserved by *TESS* (with clearly detectable transits as shown by this effort). Assuming *TESS* will reobserve all *K2* systems throughout its extended missions, we expect to be able to update the ephemerides for around half of *K2* planets (~ 250 planets) with transits deep enough to be detected by *TESS*, based on this study. Over the next couple of years, we plan to reanalyze the remaining *K2* systems with current *TESS* overlap, providing the updated parameters to the community. In future batches, we will place a focus on systems that are potentially well suited as JWST targets for atmospheric studies based on their TSMs. While we do not see
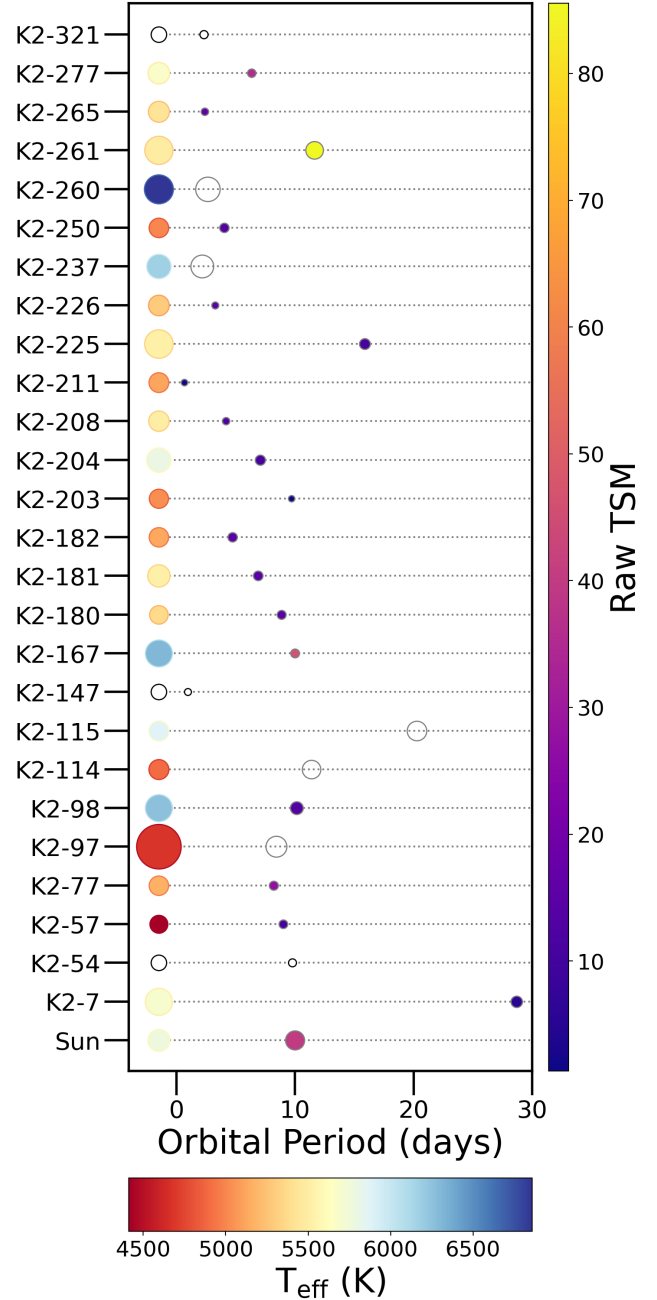
Figure 8. Architecture for each system showing the values from the global fits for the 26 systems in this analysis. The host stars are the left-most circles, with their temperatures indicated by color and relative radius shown by size. The right-most circles represent the planets, with size showing relative radius and color indicating their raw Transmission Spectroscopy Metric (TSM). The radius of the star and planet within each system is not scaled to each other. Systems for which we did not fit stellar parameters and planets that do not have a calculated TSM are represented by empty circles (see §4.2). An example of the Sun hosting a Jupiter planet with a 10-day period and TSM of 40 is shown.
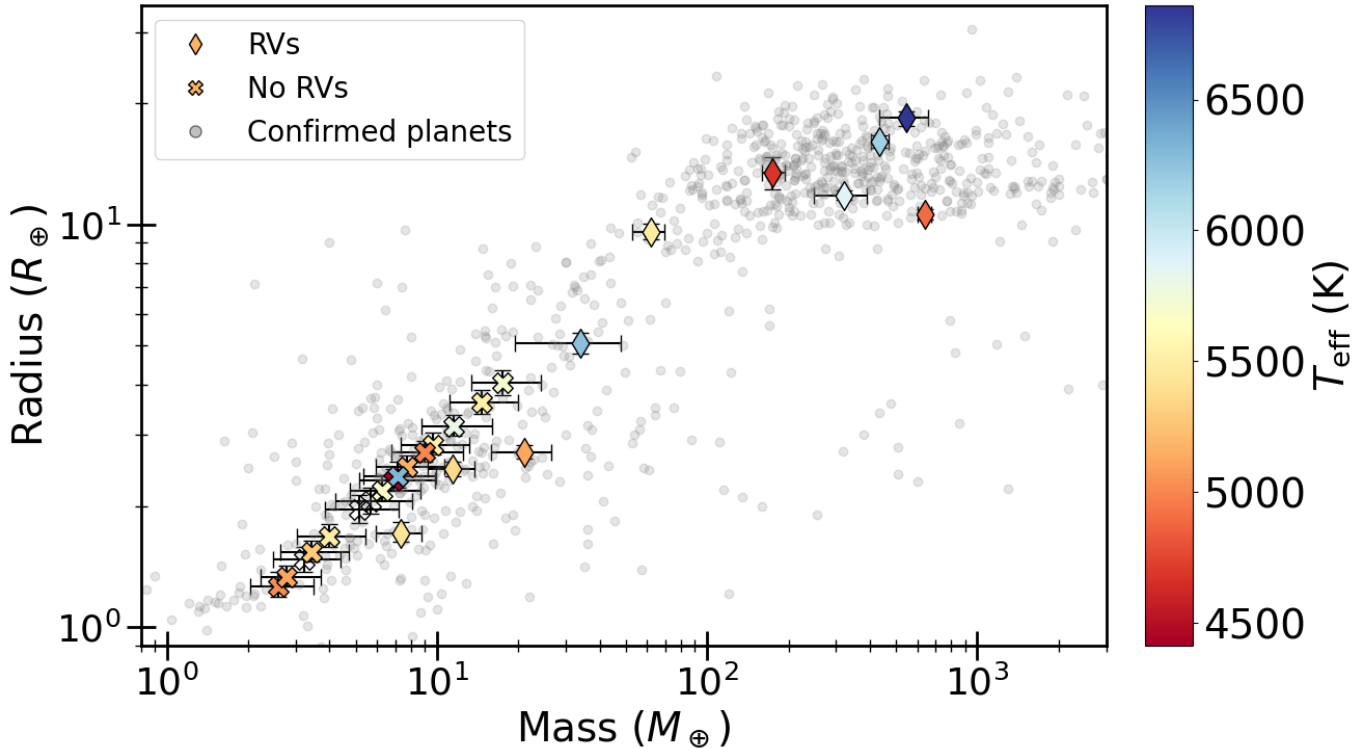
Figure 9. Radius versus mass for all confirmed exoplanets (gray; values taken from the NEA) and those in our work (using the median values from the EXOFASTv2 output). The 10 systems with planetary masses measured through RVs are indicated by diamonds, while the planets without RVs that have masses obtained from the Chen & Kipping (2017) mass-radius relations are shown as crosses. The points are colored by the effective temperature of the host star, and are empty for the three systems without fitted stellar parameters.

strong evidence for TTVs in the current work, we will make note of this in future for any systems with significant change in ephemeris, particularly for known multi-planet systems where this would be more readily detectable.

5. CONCLUSION

Past efforts to create and analyze homogeneous populations of exoplanet parameters have led to great insight into major questions in planetary formation and evolution (Wang et al. 2014; Fulton et al. 2017; Fulton & Petigura 2018). The *K2* & *TESS* Synergy is uniting NASA's planet hunting missions, and focuses on extending the scientific output of both telescopes by creating a self-consistent catalog for the *K2* and *TESS* sample while providing the community with updated ephemerides to efficiently schedule future characterization observations with facilities like JWST (Gardner et al. 2006). As well as refreshing stale ephemerides, this provides a uniform way of addressing any inconsistencies between the original *K2* ephemeris and the updated value from *TESS*. In this paper, we have presented updated parameters for 26 single-planet systems originally discovered by *K2* and more recently reobserved by *TESS* during its primary and extended missions. Following from the success of the pilot study (Ikwut-Ukwa et al. 2020), we have significantly reduced the uncertainties on transit times for the 13 systems

with transits detectable in *TESS* from hours down to minutes through the JWST operations window (∼2030). Assuming the current sample is representative of the entire *K2* catalog, we expect significant improvement on ephemerides for about half of the systems revisited by *TESS*, with the goal of a ∼250-system catalog of parameters that will be publicly available. As *TESS* continues to reobserve large portions of the entire sky during its current and possible future extended missions, there will be a well-suited opportunity to conduct this analysis on all known exoplanets, possibly leading to key insights into the evolutionary processes of exoplanets.

Software: Lightkurve (Lightkurve Collaboration et al. 2018), EXOFASTv2 (Eastman et al. 2013, 2019)

Facilities: *TESS*, *K2*, Keck (HIRES), Lick Observatory 2.4 m (Levy), Nordic Optical 2.56 m (FIES), La Silla 3.6 m (HARPS), Telescopio Nazionale Gailieo 3.58 m (HARPS-N), La Silla 1.2 m (CORALIE), FLWO 1.5m (Tillinghast Reflector Echelle Spectrograph).

REFERENCES

Adams, E. R., Jackson, B., Johnson, S., et al. 2021, Planetary Science Journal, 2, 152

Aigrain, S., Parviainen, H., & Pope, B. J. S. 2016, MNRAS, 459, 2408

Akana Murphy, J. M., Kosiarek, M. R., Batalha, N. M., et al. 2021, AJ, 162, 294

Barragán, O., Grziwa, S., Gandolfi, D., et al. 2016, AJ, 152, 193

Barros, S. C. C., Demangeon, O., & Deleuil, M. 2016, A&A, 594, A100

Bastien, F. A., Stassun, K. G., Basri, G., & Pepper, J. 2013, Nature, 500, 427

Beichman, C., Ygouf, M., Llop Sayson, J., et al. 2020, PASP, 132, 015002

Berger, T. A., Huber, D., Gaidos, E., van Saders, J. L., & Weiss, L. M. 2020a, AJ, 160, 108

Berger, T. A., Huber, D., van Saders, J. L., et al. 2020b, AJ, 159, 280

Borucki, W. J., Koch, D., Basri, G., et al. 2010, Science, 327, 977

Caldwell, D. A., Tenenbaum, P., Twicken, J. D., et al. 2020, Research Notes of the American Astronomical Society, 4, 201

Carrión-González, Ó., García Muñoz, A., Santos, N. C., et al. 2021, A&A, 651, A7

Castro González, A., Díez Alonso, E., Menéndez Blanco, J., et al. 2020, MNRAS, 499, 5416

Chen, J., & Kipping, D. 2017, ApJ, 834, 17

Choi, J., Dotter, A., Conroy, C., et al. 2016, ApJ, 823, 102

Claret, A. 2017, A&A, 600, A30

Claret, A., & Bloemen, S. 2011, A&A, 529, A75

Collins, K. A., Collins, K. I., Pepper, J., et al. 2018, AJ, 156, 234

Cosentino, R., Lovis, C., Pepe, F., et al. 2012, in Ground-based and Airborne Instrumentation for Astronomy IV, ed. I. S. McLean, S. K. Ramsay, & H. Takami, Vol. 8446, International Society for Optics and Photonics (SPIE), 657 – 676

Crossfield, I. J. M., Ciardi, D. R., Petigura, E. A., et al. 2016, ApJS, 226, 7

Cutri, R. M., Wright, E. L., T., C., & at al. 2012, VizieR Online Data Catalog, 2311, 0

Cutri, R. M., Skrutskie, M. F., van Dyk, S., et al. 2003, VizieR Online Data Catalog, 2246, 0

Dattilo, A., Vanderburg, A., Shallue, C. J., et al. 2019, AJ, 157, 169

Dotter, A. 2016, ApJS, 222, 8

Dragomir, D., Harris, M., Pepper, J., et al. 2020, AJ, 159, 219

Eastman, J. 2017, EXOFASTv2: Generalized publication-quality exoplanet modeling code, Astrophysics Source Code Library, ascl:1710.003

Eastman, J., Gaudi, B. S., & Agol, E. 2013, PASP, 125, 83

Eastman, J. D., Rodriguez, J. E., Agol, E., et al. 2019, arXiv e-prints, arXiv:1907.09480

Edwards, B., Changeat, Q., Hou Yip, K., et al. 2019, in EPSC-DPS Joint Meeting 2019, Vol. 2019, EPSC–DPS2019–595

Edwards, B., Anisman, L., Changeat, Q., et al. 2020, Research Notes of the American Astronomical Society, 4, 109

Edwards, B., Ho, C., Osborne, H., et al. 2021, ATOM - Astronomy: Theory, 2, 25

Espinoza, N., Kossakowski, D., & Brahm, R. 2019, MNRAS, 490, 2262

Fűrész, G. 2008, PhD thesis, University of Szeged, Hungary

Foreman-Mackey, D., Luger, R., Agol, E., et al. 2021, The Journal of Open Source Software, 6, 3285

Frandsen, S., & Lindberg, B. 1999, in Astrophysics with the NOT, ed. H. Karttunen & V. Piirola, 71

Fulton, B. J., & Petigura, E. A. 2018, AJ, 156, 264

Fulton, B. J., Petigura, E. A., Howard, A. W., et al. 2017, AJ, 154, 109

Gaia Collaboration, Prusti, T., de Bruijne, J. H. J., et al. 2016, A&A, 595, A1

Gaia Collaboration, Brown, A. G. A., Vallenari, A., et al. 2018, A&A, 616, A1

—. 2021, A&A, 649, A1

Gaidos, E., Mann, A. W., Rizzuto, A., et al. 2017, MNRAS, 464, 850

Gardner, J. P., Mather, J. C., Clampin, M., et al. 2006, SSRv, 123, 485

Grunblatt, S. K., Huber, D., Gaidos, E. J., et al. 2016, AJ, 152, 185

Grunblatt, S. K., Huber, D., Gaidos, E., et al. 2018, ApJL, 861, L5

Günther, M. N., & Daylan, T. 2021, ApJS, 254, 13

Hirano, T., Dai, F., Gandolfi, D., et al. 2018, AJ, 155, 127

Howell, S. B., Sobeck, C., Haas, M., et al. 2014, PASP, 126, 398

Huber, D., Bryson, S. T., Haas, M. R., et al. 2016, ApJS, 224, 2

Ikwut-Ukwa, M., Rodriguez, J. E., Bieryla, A., et al. 2020, AJ, 160, 209

Jenkins, J. M., Twicken, J. D., McCauliff, S., et al. 2016, in Proc. SPIE, Vol. 9913, Software and Cyberinfrastructure for Astronomy IV, 99133E

Johns, M., McCarthy, P., Raybould, K., et al. 2012, in Society of Photo-Optical Instrumentation Engineers (SPIE) Conference Series, Vol. 8444, Ground-based and Airborne Telescopes IV, ed. L. M. Stepp, R. Gilmozzi, & H. J. Hall, 84441H

Johnson, M. C., Dai, F., Justesen, A. B., et al. 2018a, MNRAS, 481, 596

Johnson, M. C., Rodriguez, J. E., Zhou, G., et al. 2018b, AJ, 155, 100

Kempton, E. M. R., Bean, J. L., Louie, D. R., et al. 2018, PASP, 130, 114401

Kokori, A., Tsiaras, A., Edwards, B., et al. 2021, Experimental Astronomy, arXiv:2012.07478

—. 2022, ApJS, 258, 40

Korth, J., Csizmadia, S., Gandolfi, D., et al. 2019, MNRAS, 482, 1807

Kruse, E., Agol, E., Luger, R., & Foreman-Mackey, D. 2019, ApJS, 244, 11

Lam, K. W. F., Santerne, A., Sousa, S. G., et al. 2018, A&A, 620, A77

Lightkurve Collaboration, Cardoso, J. V. d. M. a., Hedges, C., et al. 2018, Lightkurve: Kepler and TESS time series analysis in Python, ascl:1812.013

Lindegren, L., Hernández, J., Bombrun, A., et al. 2018, A&A, 616, A2

Lindegren, L., Bastian, U., Biermann, M., et al. 2021, A&A, 649, A4

Livingston, J. H., Endl, M., Dai, F., et al. 2018a, AJ, 156, 78

Livingston, J. H., Crossfield, I. J. M., Petigura, E. A., et al. 2018b, AJ, 156, 277

Luger, R., Agol, E., Kruse, E., et al. 2016, AJ, 152, 100

Lund, M. N., Handberg, R., Davies, G. R., Chaplin, W. J., & Jones, C. D. 2015, ApJ, 806, 30

Mann, A. W., Feiden, G. A., Gaidos, E., Boyajian, T., & von Braun, K. 2015, ApJ, 804, 64

Mann, A. W., Dupuy, T., Kraus, A. L., et al. 2019, ApJ, 871, 63

Mayo, A. W., Vanderburg, A., Latham, D. W., et al. 2018, AJ, 155, 136

Mayor, M., Pepe, F., Queloz, D., et al. 2003, The Messenger, 114, 20

Montet, B. T., Morton, T. D., Foreman-Mackey, D., et al. 2015, ApJ, 809, 25

Patel, J. A., & Espinoza, N. 2022, AJ, 163, 228

Paxton, B., Bildsten, L., Dotter, A., et al. 2011, ApJS, 192, 3

Paxton, B., Cantiello, M., Arras, P., et al. 2013, ApJS, 208, 4

Paxton, B., Marchant, P., Schwab, J., et al. 2015, ApJS, 220, 15

Pope, B. J. S., Parviainen, H., & Aigrain, S. 2016, MNRAS, 461, 3399

Pope, B. J. S., White, T. R., Farr, W. M., et al. 2019, ApJS, 245, 8

Queloz, D., Mayor, M., Weber, L., et al. 2000, A&A, 354, 99

Rampalli, R., Vanderburg, A., Bieryla, A., et al. 2019, AJ, 158, 62

Ricker, G. R., Winn, J. N., Vanderspek, R., et al. 2015, Journal of Astronomical Telescopes, Instruments, and Systems, 1, 014003

Rodriguez, J. E., Quinn, S. N., Vanderburg, A., et al. 2022, arXiv e-prints, arXiv:2205.05709

Schlafly, E. F., & Finkbeiner, D. P. 2011, ApJ, 737, 103

Schlegel, D. J., Finkbeiner, D. P., & Davis, M. 1998, ApJ, 500, 525

Shallue, C. J., & Vanderburg, A. 2018, AJ, 155, 94

Shporer, A., Zhou, G., Fulton, B. J., et al. 2017, AJ, 154, 188

Smith, A. M. S., Csizmadia, S., Gandolfi, D., et al. 2019, AcA, 69, 135

Smith, J. C., Stumpe, M. C., Van Cleve, J. E., et al. 2012, PASP, 124, 1000

Soto, M. G., Díaz, M. R., Jenkins, J. S., et al. 2018, MNRAS, 478, 5356

Stassun, K. G., Oelkers, R. J., Pepper, J., et al. 2018, AJ, 156, 102

Stumpe, M. C., Smith, J. C., Catanzarite, J. H., et al. 2014, PASP, 126, 100

Stumpe, M. C., Smith, J. C., Van Cleve, J. E., et al. 2012, PASP, 124, 985

Tinetti, G., Drossart, P., Eccleston, P., et al. 2018, Experimental Astronomy, 46, 135

Tinetti, G., Eccleston, P., Haswell, C., et al. 2021, arXiv e-prints, arXiv:2104.04824

Udry, S., Lovis, C., Bouchy, F., et al. 2014, arXiv e-prints, arXiv:1412.1048

Vanderburg, A., & Johnson, J. A. 2014, PASP, 126, 948

Vanderburg, A., Latham, D. W., Buchhave, L. A., et al. 2016, ApJS, 222, 14

Vanderburg, A., Huang, C. X., Rodriguez, J. E., et al. 2019, ApJL, 881, L19

Vogt, S. S., Allen, S. L., Bigelow, B. C., et al. 1994, in Proc. SPIE, Vol. 2198, Instrumentation in Astronomy VIII, ed. D. L. Crawford & E. R. Craine, 362

Wang, J., Xie, J.-W., Barclay, T., & Fischer, D. A. 2014, ApJ, 783, 4

Zellem, R., Biferno, A., Ciardi, D. R., et al. 2019, BAAS, 51, 416

Zellem, R. T., Pearson, K. A., Blaser, E., et al. 2020, PASP, 132, 054401

Zink, J. K., Hardegree-Ullman, K. K., Christiansen, J. L., et al. 2021, AJ, 162, 259

APPENDIX

A. ADDITIONAL TABLES

Table 5. Median values and 68% confidence intervals.

Priors:		K2-7	K2-54′	K2-57	K2-77	K2-97	K2-98
π	Gaia Parallax (mas)	$\mathcal{G}[1.45113, 0.02810]$	—	$\mathcal{G}[3.81841, 0.02910]$	$\mathcal{G}[7.11086, 0.04290]$	$\mathcal{G}[1.24110, 0.06320]$	$\mathcal{G}[1.94998, 0.04160]$
[Fe/H]	Metallicity (dex)	$\mathcal{G}[-0.153, 0.24]^*$	—	$\mathcal{G}[-0.01, 0.20]^*$	$\mathcal{G}[0.118, 0.080]$	$\mathcal{G}[0.267, 0.080]$	$\mathcal{G}[-0.104, 0.080]$
A_V	V-band extinction (mag)	$\mathcal{U}[0, 0.12741]$	—	$\mathcal{U}[0, 0.1209]$	$\mathcal{U}[0, 1.11693]$	$\mathcal{U}[0, 0.13733]$	$\mathcal{U}[0, 0.14477]$
$D_T^\star$	Dilution in *TESS*	$\mathcal{G}[0, 0.00030159]$	—	—	$\mathcal{G}[0, 0.00023943]$	—	$\mathcal{G}[0, 0.0018889]$
Parameter	Units	Values					
Stellar Parameters:							
M_*	Mass ($M_\odot$)	$1.056^{+0.098}_{-0.068}$	0.615 ± 0.031	$0.699^{+0.034}_{-0.031}$	$0.847^{+0.039}_{-0.038}$	$1.17^{+0.19}_{-0.13}$	$1.246^{+0.078}_{-0.11}$
R_*	Radius ($R_\odot$)	$1.533^{+0.082}_{-0.074}$	0.643 ± 0.031	$0.671^{+0.023}_{-0.022}$	$0.792^{+0.027}_{-0.025}$	$4.14^{+0.28}_{-0.26}$	$1.518^{+0.082}_{-0.076}$
L_*	Luminosity ($L_\odot$)	$2.24^{+0.12}_{-0.11}$	$0.095^{+0.034}_{-0.026}$	$0.1541^{+0.0053}_{-0.0051}$	$0.401^{+0.04}_{-0.037}$	$7.36^{+0.83}_{-0.72}$	$3.19^{+0.23}_{-0.21}$
F_{Bol}	Bolometric Flux (cgs)	$1.504e-10^{+5.1e-12}_{-5.5e-12}$	—	$7.18e-11^{+2.2e-12}_{-2.1e-12}$	$6.47e-10^{+6.3e-11}_{-5.9e-11}$	$3.521e-10^{+9.9e-12}_{-1e-11}$	$3.88e-10^{+2.2e-11}_{-2e-11}$
ρ_*	Density (cgs)	$0.416^{+0.086}_{-0.074}$	$3.25^{+0.54}_{-0.45}$	$3.26^{+0.32}_{-0.29}$	$2.41^{+0.25}_{-0.24}$	$0.0235^{+0.0065}_{-0.0048}$	$0.499^{+0.1}_{-0.087}$
$\log g$	Surface gravity (cgs)	$4.092^{+0.065}_{-0.062}$	4.61 ± 0.047	4.629 ± 0.028	$4.569^{+0.03}_{-0.033}$	$3.276^{+0.085}_{-0.077}$	$4.169^{+0.06}_{-0.063}$
$T_{\rm eff}$	Effective Temperature (K)	5700.0 ± 140.0	3990.0 ± 300.0	4413.0 ± 76.0	5160.0 ± 130.0	$4673.0^{+170.0}_{-93.0}$	$6260.0^{+170.0}_{-160.0}$
[Fe/H]	Metallicity (dex)	$0.049^{+0.120}_{-0.081}$	$-0.02^{+0.95}_{-0.99}$	$0.08^{+0.2}_{-0.14}$	$0.13^{+0.078}_{-0.076}$	$0.328^{+0.079}_{-0.081}$	$-0.044^{+0.064}_{-0.07}$
[Fe/H]$_0$	Initial Metallicity[1]	$0.103^{+0.100}_{-0.082}$	—	$0.07^{+0.18}_{-0.13}$	$0.115^{+0.08}_{-0.078}$	$0.261^{+0.074}_{-0.078}$	$0.069^{+0.062}_{-0.065}$
Age	Age (Gyr)	$8.6^{+2.5}_{-3.1}$	—	$6.8^{+4.7}_{-4.5}$	$4.7^{+5.2}_{-3.4}$	$7.5^{+4.0}_{-3.2}$	$3.4^{+2.2}_{-1.4}$
EEP	Equal Evolutionary Phase[2]	$447.5^{+8.7}_{-24.0}$	—	$327.0^{+14.0}_{-30.0}$	$334.0^{+19.0}_{-37.0}$	$499.6^{+8.7}_{-9.6}$	$389.0^{+41.0}_{-42.0}$
A_V	V-band extinction (mag)	$0.087^{+0.029}_{-0.047}$	—	$0.063^{+0.04}_{-0.042}$	$0.59^{+0.14}_{-0.15}$	$0.091^{+0.034}_{-0.051}$	$0.088^{+0.041}_{-0.055}$
σ_{SED}	SED photometry error scaling	$0.6^{+0.26}_{-0.15}$	—	$1.45^{+0.73}_{-0.39}$	$0.9^{+0.4}_{-0.24}$	$0.9^{+0.38}_{-0.24}$	$1.13^{+0.54}_{-0.3}$
ϖ	Parallax (mas)	1.449 ± 0.028	—	3.818 ± 0.03	7.107 ± 0.043	1.222 ± 0.062	1.951 ± 0.042
d	Distance (pc)	$689.0^{+14.0}_{-13.0}$	—	$261.9^{+2.1}_{-2.0}$	$140.71^{+0.85}_{-0.84}$	$818.0^{+44.0}_{-40.0}$	512.0 ± 11.0
Planetary Parameters:							
P	Period (days)	$28.6781^{+0.0046}_{-0.0051}$	$9.7833^{+0.0013}_{-0.0012}$	$9.0073^{+0.0012}_{-0.0011}$	$8.2000844^{+8.6e-06}_{-7.3e-06}$	$8.407115 \pm 2.3e-05$	$10.1367349^{+9.4e-06}_{-9.2e-06}$
R_P	Radius (R_J)	$0.360^{+0.027}_{-0.023}$	$0.233^{+0.019}_{-0.017}$	$0.206^{+0.015}_{-0.012}$	$0.223^{+0.015}_{-0.011}$	1.2 ± 0.11	$0.452^{+0.028}_{-0.025}$
M_P	Mass (M_J)	$0.055^{+0.021}_{-0.013}$	$0.0264^{+0.0100}_{-0.0066}$	$0.0217^{+0.0091}_{-0.0055}$	$0.0244^{+0.0091}_{-0.0058}$	$0.549^{+0.059}_{-0.046}$	$0.107^{+0.044}_{-0.046}$
T_C	Time of conjunction[3] (BJD$_{\rm TDB}$)	$2456824.6164^{+0.0079}_{-0.0067}$	$2456982.9376^{+0.0044}_{-0.0045}$	$2456984.335^{+0.0037}_{-0.0039}$	2457070.8051 ± 0.001	2457142.0537 ± 0.0031	$2457145.97972^{+0.00092}_{-0.00091}$
T_T	Time of minimum projected separation[4] (BJD$_{\rm TDB}$)	$2456824.6164^{+0.0076}_{-0.0076}$	$2456982.9376^{+0.0043}_{-0.0044}$	$2456984.335^{+0.0036}_{-0.0038}$	2457070.80511 ± 0.0008	2457142.05 ± 0.0027	$2457145.97967 \pm 0.00084$
T_0	Optimal conjunction Time[5] (BJD$_{\rm TDB}$)	$2456853.2946^{+0.0046}_{-0.0042}$	$2457012.2875^{+0.0028}_{-0.0027}$	2457011.3568 ± 0.0023	$2457316.80766^{+0.00099}_{-0.00096}$	$2457722.1447^{+0.0027}_{-0.0026}$	$2457662.95321^{+0.00077}_{-0.00074}$
a	Semi-major axis (AU)	$0.1867^{+0.0056}_{-0.0041}$	0.0761 ± 0.0013	$0.0752^{+0.0012}_{-0.0011}$	0.0753 ± 0.0011	$0.0854^{+0.0044}_{-0.0033}$	$0.0986^{+0.002}_{-0.0029}$
i	Inclination (Degrees)	$89.08^{+0.58}_{-0.47}$	$89.08^{+0.59}_{-0.5}$	$88.95^{+0.67}_{-0.46}$	$88.33^{+0.83}_{-0.37}$	$75.5^{+1.6}_{-1.8}$	$88.39^{+0.98}_{-0.74}$
e	Eccentricity	$0.24^{+0.40}_{-0.17}$	$0.24^{+0.40}_{-0.18}$	$0.25^{+0.38}_{-0.17}$	$0.29^{+0.37}_{-0.19}$	$0.207^{+0.039}_{-0.038}$	$0.119^{+0.15}_{-0.083}$
ω_*	Argument of Periastron (Degrees)	$-30.0^{+110.0}_{-130.0}$	$-43.0^{+93.0}_{-120.0}$	$-20.0^{+110.0}_{-140.0}$	$-40.0^{+100.0}_{-130.0}$	$68.4^{+10.0}_{-11.0}$	$14.0^{+110.0}_{-98.0}$
T_{eq}	Equilibrium temperature[6] (K)	$786.0^{+14.0}_{-14.0}$	$560.0^{+45.0}_{-44.0}$	$635.8^{+6.8}_{-6.7}$	806.0 ± 18.0	$1566.0^{+49.0}_{-50.0}$	$1185.0^{+23.0}_{-21.0}$
$\tau_{\rm circ}$	Tidal circularization timescale (Gyr)	$28000.0^{+35000.0}_{-27000.0}$	$750.0^{+1000.0}_{-740.0}$	$880.0^{+1000.0}_{-860.0}$	$380.0^{+580.0}_{-380.0}$	$4.5^{+3.2}_{-1.8}$	$330.0^{+300.0}_{-220.0}$
K	RV semi-amplitude (m/s)	$3.9^{+2.0}_{-1.1}$	$3.8^{+2.1}_{-1.1}$	$2.98^{+1.7}_{-0.83}$	$3.09^{+1.5}_{-0.83}$	48.7 ± 2.3	$8.8^{+3.5}_{-3.8}$
R_P/R_*	Radius of planet in stellar radii	$0.02408^{+0.0011}_{-0.0009}$	$0.0373^{+0.0023}_{-0.0020}$	$0.0315^{+0.0019}_{-0.0014}$	$0.0288^{+0.0016}_{-0.0011}$	0.0298 ± 0.0011	$0.03049^{+0.0007}_{-0.00044}$
a/R_*	Semi-major axis in stellar radii	$26.3^{+1.7}_{-1.6}$	$25.4^{+1.3}_{-1.1}$	$24.09^{+0.76}_{-0.73}$	$20.46^{+0.68}_{-0.69}$	$4.44^{+0.38}_{-0.34}$	$13.94^{+0.9}_{-0.87}$
δ	$(R_P/R_*)^2$	$0.00058^{+5.4e-05}_{-4.3e-05}$	$0.00139^{+0.00018}_{-0.00014}$	$0.00099^{+0.00012}_{-8.3e-05}$	$0.00081^{+9.7e-05}_{-6e-05}$	$0.000891^{+6.7e-05}_{-6.2e-05}$	$0.00093^{+4.3e-05}_{-2.7e-05}$
$Depth_{K2}$	Flux decrement at mid transit for *K2*	$0.000693 \pm 4.5e-05$	$0.00169^{+0.00019}_{-0.00017}$	$0.001377^{+9.7e-05}_{-0.0001}$	$0.000995^{+4e-05}_{-4.6e-05}$	$0.000576^{+5.6e-05}_{-6.4e-05}$	$0.00108^{+2.1e-05}_{-2e-05}$
$Depth_{TESS}$	Flux decrement at mid transit for *TESS*	—	—	—	$0.00096 \pm 3e-05$	$0.000681^{+3.5e-05}_{-3.9e-05}$	$0.001035 \pm 2.4e-05$
τ	Ingress/egress transit duration (days)	$0.0085^{+0.0036}_{-0.0012}$	$0.00476^{+0.0023}_{-0.00066}$	$0.00382^{+0.0017}_{-0.00059}$	$0.0042^{+0.0026}_{-0.0012}$	$0.0348^{+0.0087}_{-0.0073}$	$0.00729^{+0.0021}_{-0.00096}$
T_{14}	Total transit duration (days)	$0.3159^{+0.0096}_{-0.0093}$	$0.1162^{+0.0074}_{-0.0072}$	$0.1075^{+0.0056}_{-0.006}$	$0.106^{+0.0028}_{-0.0023}$	$0.2613^{+0.0077}_{-0.0072}$	$0.2134^{+0.0024}_{-0.0021}$
b	Transit Impact parameter	$0.37^{+0.24}_{-0.25}$	$0.37^{+0.26}_{-0.25}$	$0.39^{+0.24}_{-0.26}$	$0.55^{+0.19}_{-0.33}$	$0.895^{+0.02}_{-0.026}$	$0.37^{+0.19}_{-0.24}$
ρ_P	Density (cgs)	$1.45^{+0.53}_{-0.35}$	$2.55^{+0.95}_{-0.62}$	$3.04^{+1.2}_{-0.74}$	$2.69^{+0.97}_{-0.63}$	$0.392^{+0.14}_{-0.1}$	$1.4^{+0.71}_{-0.64}$
$logg_P$	Surface gravity	$3.02^{+0.13}_{-0.11}$	$3.08^{+0.13}_{-0.12}$	$3.1^{+0.14}_{-0.12}$	$3.08^{+0.13}_{-0.11}$	$2.974^{+0.095}_{-0.091}$	$3.12^{+0.16}_{-0.22}$
T_S	Time of eclipse (BJD$_{\rm TDB}$)	$2456810.3^{+6.7}_{-6.4}$	2456987.8 ± 2.2	2456979.8 ± 2.1	$2457066.7^{+2.1}_{-2.0}$	$2457138.26^{+0.14}_{-0.15}$	$2457141.05^{+0.93}_{-0.61}$
$T_{S,14}$	Total eclipse duration (days)	$0.305^{+0.060}_{-0.096}$	$0.108^{+0.02}_{-0.037}$	$0.105^{+0.022}_{-0.032}$	$0.103^{+0.028}_{-0.03}$	0.0 ± 0.0	$0.217^{+0.036}_{-0.027}$
$e\cos\omega_*$	....	$0.0^{+0.37}_{-0.35}$	$0.0^{+0.34}_{-0.35}$	0.0 ± 0.37	$0.0^{+0.4}_{-0.39}$	$0.075^{+0.025}_{-0.027}$	$0.021^{+0.14}_{-0.094}$
$e\sin\omega_*$	....	$-0.02^{+0.10}_{-0.27}$	$-0.04^{+0.10}_{-0.29}$	$-0.01^{+0.11}_{-0.26}$	$-0.02^{+0.16}_{-0.3}$	$0.191^{+0.045}_{-0.046}$	$0.008^{+0.086}_{-0.1}$
M_P/M_*	Mass ratio	$4.9e-05^{+2.0e-05}_{-1.3e-05}$	$4.1E-05^{+1.7E-05}_{-1E-05}$	$2.96e-05^{+1e-05}_{-7.5e-06}$	$2.75e-05^{+1.2e-05}_{-6.6e-06}$	$0.000444^{+2.9e-05}_{-3e-05}$	$8.2e-05^{+3.3e-05}_{-3.5e-05}$
d/R_*	Separation at mid transit	$24.2^{+4.3}_{-5.7}$	$24.2^{+3.9}_{-5.3}$	$21.9^{+3.3}_{-4.7}$	$18.1^{+3.9}_{-4.1}$	$3.57^{+0.38}_{-0.34}$	$13.5^{+1.7}_{-2.0}$

Table 5 *continued*

Table 5 *(continued)*

Notes. See Table 3 in Eastman et al. (2019) for a detailed description of all parameters. Gaussian and uniform priors are indicated as $\mathcal{G}$[median, width] and $\mathcal{U}$[lower bound, upper bound], respectively. Metallicity priors are adopted from TRES spectra unless otherwise indicated. * Gaussian priors were placed on dilution in *TESS* only for systems with a contamination listed on EXOFOP. $'$ The stellar parameters from the global fit are not considered reliable as the SED was not included within this fit. * From Huber et al. (2016).

[1]The metallicity of the star at birth. [2]Corresponds to static points in a star's evolutionary history. See §2 in Dotter (2016). [3]Time of conjunction is commonly reported as the "transit time". [4]Time of minimum projected separation is a more correct "transit time". [5]Optimal time of conjunction minimizes the covariance between T_C and Period. [6]Assumes no albedo and perfect redistribution.

Table 6. Median values and 68% confidence intervals.

Priors:		K2-114	K2-115	K2-147′	K2-167	K2-180
π	Gaia Parallax (mas)	$\mathcal{G}[2.12963, 0.03560]$	$\mathcal{G}[2.49675, 0.02480]$	—	$\mathcal{G}[12.45657, 0.07130]$	$\mathcal{G}[4.93626, 0.04120]$
[Fe/H]	Metallicity (dex)	$\mathcal{G}[0.401, 0.037]^{\dagger}$	$\mathcal{G}[-0.23, 0.04]^{*}$	—	$\mathcal{G}[-0.459, 0.080]$	$\mathcal{G}[-0.588, 0.080]$
A_V	V-band extinction (mag)	$\mathcal{U}[0, 0.08928]$	$\mathcal{U}[0, 1.302]$	—	$\mathcal{U}[0, 0.12431]$	$\mathcal{U}[0, 0.08866]$
D^{*}_{T}	Dilution in *TESS*	—	$\mathcal{G}[0, 1.40623e-05]$	—	$\mathcal{G}[0, 2.69843e-05]$	$\mathcal{G}[0, 0.040635]$

Parameter	Units	Values				
Stellar Parameters:						
M_*	Mass ($M_\odot$)	$0.863^{+0.037}_{-0.031}$	$0.918^{+0.039}_{-0.046}$	0.563 ± 0.028	$1.084^{+0.1}_{-0.097}$	$0.735^{+0.035}_{-0.029}$
R_*	Radius ($R_\odot$)	$0.832^{+0.022}_{-0.021}$	$0.855^{+0.024}_{-0.021}$	0.578 ± 0.028	$1.499^{+0.077}_{-0.071}$	$0.719^{+0.025}_{-0.023}$
L_*	Luminosity ($L_\odot$)	0.36 ± 0.015	$0.78^{+0.1}_{-0.071}$	$0.056^{+0.022}_{-0.017}$	3.21 ± 0.14	0.386 ± 0.014
F_{Bol}	Bolometric Flux (cgs)	$5.18e-11 \pm 1.4e-12$	$1.55e-10^{+2e-11}_{-1.4e-11}$	—	$1.594e-08^{+6.6e-10}_{-6.7e-10}$	$3.011e-10^{+9.6e-12}_{-9.7e-12}$
ρ_*	Density (cgs)	$2.11^{+0.18}_{-0.17}$	$2.08^{+0.16}_{-0.19}$	$4.11^{+0.71}_{-0.58}$	$0.454^{+0.098}_{-0.086}$	$2.79^{+0.31}_{-0.28}$
$\log g$	Surface gravity (cgs)	$4.534^{+0.027}_{-0.026}$	$4.538^{+0.024}_{-0.033}$	4.665 ± 0.048	$4.122^{+0.066}_{-0.072}$	$4.591^{+0.034}_{-0.033}$
$T_{\rm eff}$	Effective Temperature (K)	$4899.0^{+59.0}_{-58.0}$	$5870.0^{+170.0}_{-150.0}$	3690.0 ± 300.0	6310.0 ± 170.0	$5365.0 \pm +92.0$
[Fe/H]	Metallicity (dex)	$0.42^{+0.036}_{-0.037}$	$-0.198^{+0.043}_{-0.049}$	$-0.02^{+0.96}_{-1.0}$	-0.456 ± 0.081	$-0.578^{+0.079}_{-0.080}$
$[\rm Fe/H]_0$	Initial Metallicity[1]	0.39 ± 0.046	$-0.202^{+0.056}_{-0.058}$	—	$-0.253^{+0.075}_{-0.088}$	$-0.531^{+0.085}_{-0.086}$
Age	Age (Gyr)	$7.6^{+4.2}_{-4.6}$	$2.2^{+3.5}_{-1.6}$	—	$5.3^{+2.5}_{-2.0}$	$7.5^{+4.4}_{-4.7}$
EEP	Equal Evolutionary Phase[2]	$348.0^{+23.0}_{-26.0}$	$325.0^{+24.0}_{-39.0}$	—	$431.0^{+16.0}_{-39.0}$	$345.0^{+16.0}_{-25.0}$
A_V	V-band extinction (mag)	$0.05^{+0.027}_{-0.032}$	$0.17^{+0.13}_{-0.11}$	—	$0.07^{+0.038}_{-0.045}$	$0.051^{+0.027}_{-0.032}$
σ_{SED}	SED photometry error scaling	$1.09^{+0.48}_{-0.29}$	$1.13^{+0.5}_{-0.32}$	—	$1.65^{+0.59}_{-0.37}$	$1.48^{+0.58}_{-0.35}$
ϖ	Parallax (mas)	$2.122^{+0.035}_{-0.034}$	2.496 ± 0.025	—	12.456 ± 0.071	$4.937^{+0.042}_{-0.041}$
d	Distance (pc)	$471.2^{+7.8}_{-7.6}$	$400.7^{+4.0}_{-3.9}$	—	80.29 ± 0.46	202.6 ± 1.7
Planetary Parameters:						
P	Period (days)	$11.390931^{+3.1e-06}_{-3.2e-06}$	$20.2729914 \pm 5e-06$	$0.961939 \pm 2.9e-05$	$9.978541^{+2.3e-05}_{-1.9e-05}$	$8.865663^{+1.1e-05}_{-1e-05}$
R_P	Radius (R_J)	$0.945^{+0.029}_{-0.028}$	$1.053^{+0.03}_{-0.028}$	$0.1314^{+0.0099}_{-0.0088}$	$0.211^{+0.019}_{-0.013}$	$0.2200^{+0.0098}_{-0.0086}$
M_P	Mass (M_J)	2.01 ± 0.12	$1.01^{+0.22}_{-0.23}$	$0.0101^{+0.0037}_{-0.0056}$	$0.0224^{+0.0088}_{-0.0056}$	$0.0359^{+0.0075}_{-0.0056}$
T_C	Time of conjunction[3] (BJD$_{\rm TDB}$)	$2457140.324^{+0.00023}_{-0.00022}$	2458495.17373 ± 0.0003	$2457301.9457^{+0.0016}_{-0.0017}$	2456979.9331 ± 0.0024	$2457143.3957^{+0.00089}_{-0.00088}$
T_T	Time of minimum projected separation[4] (BJD$_{\rm TDB}$)	$2457140.32397^{+0.00023}_{-0.00022}$	$2458495.17376 \pm 0.00028$	$2457301.9457^{+0.0014}_{-0.0015}$	$2456979.9331^{+0.0016}_{-0.0015}$	$2457143.3957^{+0.00089}_{-0.00088}$
T_0	Optimal conjunction Time[5] (BJD$_{\rm TDB}$)	$2457687.08869 \pm 0.00016$	$2457522.07014 \pm 0.00017$	$2457343.30907^{+0.001}_{-0.00099}$	$2457299.2465^{+0.0022}_{-0.0023}$	$2457489.1566^{+0.00078}_{-0.00076}$
a	Semi-major axis (AU)	$0.0944^{+0.0013}_{-0.0011}$	$0.1415^{+0.002}_{-0.0024}$	$0.01575^{+0.00026}_{-0.00027}$	$0.0932^{+0.0028}_{-0.0029}$	$0.0756^{+0.0012}_{-0.001}$
i	Inclination (Degrees)	$89.16^{+0.18}_{-0.13}$	$88.912^{+0.057}_{-0.075}$	$83.6^{+3.6}_{-1.8}$	$86.8^{+1.6}_{-1.1}$	$89.15^{+0.51}_{-0.38}$
e	Eccentricity	0.079 ± 0.03	$0.063^{+0.061}_{-0.042}$	$0.38^{+0.26}_{-0.22}$	0.48 ± 0.26	$0.075^{+0.080}_{-0.051}$
ω_*	Argument of Periastron (Degrees)	$-50.0^{+22.0}_{-13.0}$	$137.0^{+46.0}_{-87.0}$	$40.0^{+100.0}_{-150.0}$	$140.0^{+120.0}_{-100.0}$	$130.0^{+120.0}_{-110.0}$
T_{eq}	Equilibrium temperature[6] (K)	$701.4^{+7.6}_{-7.7}$	$696.0^{+19.0}_{-15.0}$	$1077.0^{+93.0}_{-92.0}$	$1220.0^{+20.0}_{-19.0}$	$797.5^{+8.4}_{-8.5}$
τ_{circ}	Tidal circularization timescale (Gyr)	$256.0^{+45.0}_{-37.0}$	$960.0^{+310.0}_{-330.0}$	$0.089^{+0.24}_{-0.084}$	$270.0^{+1600.0}_{-270.0}$	$1950.0^{+750.0}_{-690.0}$
K	RV semi-amplitude (m/s)	200.0 ± 10.0	$80.0^{+17.0}_{-18.0}$	$3.44^{+1.4}_{-0.86}$	$2.44^{+1.3}_{-0.72}$	$4.36^{+0.90}_{-0.82}$
R_P/R_*	Radius of planet in stellar radii	$0.1167^{+0.0013}_{-0.0014}$	$0.12659^{+0.00075}_{-0.00084}$	$0.0234^{+0.0012}_{-0.0011}$	$0.01436^{+0.0011}_{-0.0005}$	$0.03141^{+0.00069}_{-0.00055}$
a/R_*	Semi-major axis in stellar radii	$24.4^{+0.67}_{-0.66}$	$35.62^{+0.91}_{-1.1}$	$5.86^{+0.32}_{-0.29}$	13.37 ± 0.9	$22.63^{+0.82}_{-0.79}$
δ	$(R_P/R_*)^2$	$0.01361^{+0.00031}_{-0.00033}$	$0.01603^{+0.00019}_{-0.00021}$	$0.000545^{+5.9e-05}_{-4.8e-05}$	$0.000206^{+3.1e-05}_{-1.4e-05}$	$0.000987^{+4.4e-05}_{-3.4e-05}$
$Depth_{\rm K2}$	Flux decrement at mid transit for *K2*	$0.01856^{+0.00028}_{-0.00027}$	$0.01732^{+0.00018}_{-0.00016}$	$0.0006^{+4.7e-05}_{-4.3e-05}$	$0.0002287^{+8.7e-06}_{-8.6e-06}$	$0.00121^{+3.5e-05}_{-3.4e-05}$
$Depth_{\rm TESS}$	Flux decrement at mid transit for *TESS*	$0.0171^{+0.00029}_{-0.0003}$	0.01695 ± 0.00016	—	$0.0002225^{+1.2e-05}_{-1e-05}$	$0.001152 \pm 3.4e-05$
τ	Ingress/egress transit duration (days)	0.0199 ± 0.0014	$0.0299^{+0.0014}_{-0.0015}$	$0.00114^{+0.00083}_{-0.00028}$	$0.00301^{+0.0035}_{-0.00089}$	$0.00403^{+0.00081}_{-0.00041}$
T_{14}	Total transit duration (days)	0.1654 ± 0.0012	0.1614 ± 0.0011	0.0376 ± 0.0025	$0.15^{+0.0045}_{-0.0042}$	$0.1187^{+0.0020}_{-0.0019}$
b	Transit Impact parameter	$0.378^{+0.061}_{-0.085}$	$0.655^{+0.018}_{-0.021}$	$0.5^{+0.24}_{-0.34}$	$0.55^{+0.26}_{-0.36}$	$0.33^{+0.17}_{-0.20}$
ρ_P	Density (cgs)	$2.96^{+0.34}_{-0.31}$	$1.07^{+0.26}_{-0.27}$	$5.5^{+1.9}_{-1.3}$	$2.89^{+1.1}_{-0.69}$	$4.16^{+1.10}_{-0.92}$
$logg_P$	Surface gravity	$3.748^{+0.037}_{-0.038}$	$3.356^{+0.088}_{-0.12}$	$3.16^{+0.13}_{-0.1}$	$3.09^{+0.13}_{-0.11}$	$3.263^{+0.089}_{-0.099}$
T_S	Time of eclipse (BJD$_{\rm TDB}$)	$2457134.99^{+0.11}_{-0.12}$	$2458505.03^{+0.62}_{-0.89}$	2457301.47 ± 0.26	$2456974.9^{+3.2}_{-3.3}$	$2457147.81^{+0.43}_{-0.36}$
$T_{S,14}$	Total eclipse duration (days)	$0.1493^{+0.009}_{-0.0079}$	$0.165^{+0.0043}_{-0.0038}$	$0.0399^{+0.019}_{-0.0073}$	$0.151^{+0.094}_{-0.054}$	$0.121^{+0.014}_{-0.011}$
$e \cos \omega_*$		$0.049^{+0.015}_{-0.017}$	$-0.022^{+0.048}_{-0.069}$	0.0 ± 0.43	$-0.0^{+0.5}_{-0.52}$	$-0.003^{+0.076}_{-0.063}$
$e \sin \omega_*$		$-0.058^{+0.036}_{-0.034}$	$0.024^{+0.04}_{-0.028}$	$0.09^{+0.19}_{-0.21}$	$0.1^{+0.25}_{-0.34}$	$0.011^{+0.059}_{-0.062}$
M_P/M_*	Mass ratio	0.00222 ± 0.00011	$0.00106^{+0.00022}_{-0.00024}$	$1.72e-05^{+6.4e-06}_{-4e-06}$	$1.98e-05^{+8.4e-06}_{-5.3e-06}$	$4.66e-05^{+9.6e-06}_{-8.9e-06}$
d/R_*	Separation at mid transit	25.7 ± 1.4	$34.5^{+1.9}_{-2.5}$	$4.3^{+1.5}_{-1.1}$	$8.7^{+4.7}_{-2.8}$	$22.3^{+1.8}_{-1.9}$

Notes. See Table 3 in Eastman et al. (2019) for a detailed description of all parameters. Gaussian and uniform priors are indicated as $\mathcal{G}$[median, width] and $\mathcal{U}$[lower bound, upper bound], respectively. Metallicity priors are adopted from TRES spectra unless otherwise indicated. * Gaussian priors were placed on dilution in *TESS* only for systems with a contamination listed on EXOFOP. ′ The stellar parameters from the global fit are not considered reliable as the SED was not included within this fit. † From Ikwut-Ukwa et al. (2020). * From Shporer et al. (2017).
[1]The metallicity of the star at birth. [2]Corresponds to static points in a star's evolutionary history. See §2 in Dotter (2016). [3]Time of conjunction is commonly reported as the "transit time". [4]Time of minimum projected separation is a more correct "transit time". [5]Optimal time of conjunction minimizes the covariance between T_C and Period. [6]Assumes no albedo and perfect redistribution.

Table 7. Median values and 68% confidence intervals.

Priors:		K2-181	K2-182	K2-203	K2-204	K2-208
π	Gaia Parallax (mas)	$\mathcal{G}[2.80448, 0.04020]$	$\mathcal{G}[6.50953, 0.05160]$	$\mathcal{G}[5.93701, 0.05600]$	$\mathcal{G}[1.83974, 0.05160]$	$\mathcal{G}[3.85946, 0.04790]$
[Fe/H]	Metallicity (dex)	$\mathcal{G}[0.416, 0.080]$	$\mathcal{G}[-0.006, 0.080]$	$\mathcal{G}[-0.073, 0.080]$	$\mathcal{G}[0.064, 0.080]$	$\mathcal{G}[-0.116, 0.080]$
A_V	V-band extinction (mag)	$\mathcal{U}[0, 0.10664]$	$\mathcal{U}[0, 0.086490]$	$\mathcal{U}[0, 0.13733]$	$\mathcal{U}[0, 0.10416]$	$\mathcal{U}[0, 0.08556]$
$D_T^\star$	Dilution in TESS	—	$\mathcal{G}[0, 0.00028648]$	—	—	—

Parameter	Units	Values				
Stellar Parameters:						
M_*	Mass ($M_\odot$)	$1.022^{+0.060}_{-0.058}$	$0.823^{+0.036}_{-0.033}$	$0.793^{+0.033}_{-0.029}$	$1.076^{+0.092}_{-0.086}$	$0.881^{+0.045}_{-0.042}$
R_*	Radius ($R_\odot$)	$1.04^{+0.043}_{-0.039}$	$0.789^{+0.025}_{-0.023}$	$0.765^{+0.024}_{-0.023}$	$1.253^{+0.055}_{-0.053}$	$0.872^{+0.033}_{-0.03}$
L_*	Luminosity ($L_\odot$)	$0.903^{+0.038}_{-0.036}$	$0.388^{+0.013}_{-0.012}$	0.337 ± 0.013	$1.58^{+0.11}_{-0.1}$	$0.629^{+0.027}_{-0.026}$
F_{Bol}	Bolometric Flux (cgs)	$2.267e-10^{+6.9e-12}_{-6.4e-12}$	$5.26e-10 \pm 1.5e-11$	$3.79e-10 \pm 1.3e-11$	$1.692e-10^{+6.2e-12}_{-5.7e-12}$	$2.992e-10^{+1.1e-11}_{-9.9e-12}$
ρ_*	Density (cgs)	$1.28^{+0.19}_{-0.18}$	$2.37^{+0.23}_{-0.22}$	$2.5^{+0.26}_{-0.23}$	$0.77^{+0.14}_{-0.11}$	$1.88^{+0.24}_{-0.23}$
$\log g$	Surface gravity (cgs)	$4.413^{+0.047}_{-0.050}$	$4.56^{+0.029}_{-0.032}$	4.57 ± 0.031	$4.273^{+0.056}_{-0.054}$	$4.503^{+0.04}_{-0.042}$
$T_{\rm eff}$	Effective Temperature (K)	$5520.0^{+100.0}_{-110.0}$	$5128.0^{+79.0}_{-80.0}$	$5026.0^{+82.0}_{-81.0}$	$5783.0^{+100.0}_{-98.0}$	5500.0 ± 100.0
[Fe/H]	Metallicity (dex)	0.385 ± 0.057	$0.022^{+0.077}_{-0.066}$	$-0.021^{+0.064}_{-0.041}$	$0.21^{+0.18}_{-0.19}$	-0.064 ± 0.054
[Fe/H]$_0$	Initial Metallicity[1]	$0.366^{+0.058}_{-0.060}$	$0.025^{+0.077}_{-0.071}$	$-0.01^{+0.063}_{-0.057}$	$0.23^{+0.15}_{-0.16}$	-0.048 ± 0.063
Age	Age (Gyr)	$5.9^{+4.5}_{-3.8}$	$6.2^{+4.9}_{-4.5}$	$6.9^{+4.6}_{-4.5}$	$6.5^{+3.7}_{-3.1}$	$6.1^{+4.8}_{-4.1}$
EEP	Equal Evolutionary Phase[2]	$374.0^{+36.0}_{-43.0}$	$341.0^{+19.0}_{-31.0}$	$341.0^{+15.0}_{-29.0}$	$413.0^{+20.0}_{-44.0}$	$349.0^{+35.0}_{-30.0}$
A_V	V-band extinction (mag)	$0.046^{+0.036}_{-0.030}$	$0.05^{+0.026}_{-0.032}$	$0.073^{+0.044}_{-0.047}$	$0.063^{+0.029}_{-0.038}$	$0.049^{+0.025}_{-0.032}$
σ_{SED}	SED photometry error scaling	$0.341^{+0.140}_{-0.085}$	$1.1^{+0.45}_{-0.27}$	$0.8^{+0.33}_{-0.2}$	$1.01^{+0.46}_{-0.27}$	$0.97^{+0.41}_{-0.25}$
ϖ	Parallax (mas)	2.802 ± 0.04	6.508 ± 0.052	$5.935^{+0.055}_{-0.056}$	1.83 ± 0.052	3.857 ± 0.048
d	Distance (pc)	$356.9^{+5.2}_{-5.1}$	153.7 ± 1.2	168.5 ± 1.6	$546.0^{+16.0}_{-15.0}$	259.3 ± 3.2
Planetary Parameters:						
P	Period (days)	$6.893813 \pm 1.1e-05$	$4.7369696 \pm 1.7e-06$	9.6952 ± 0.0014	$7.055908^{+5.8e-05}_{-7.4e-05}$	4.19097 ± 0.00023
R_P	Radius (R_J)	$0.253^{+0.019}_{-0.014}$	$0.242^{+0.0099}_{-0.0081}$	$0.1129^{+0.0091}_{-0.0071}$	$0.283^{+0.016}_{-0.014}$	$0.1494^{+0.011}_{-0.0082}$
M_P	Mass (M_J)	$0.0304^{+0.0110}_{-0.0073}$	$0.066^{+0.017}_{-0.016}$	$0.0081^{+0.0029}_{-0.0017}$	$0.0365^{+0.014}_{-0.0089}$	$0.0125^{+0.0046}_{-0.003}$
T_C	Time of conjunction[3] (BJD$_{\rm TDB}$)	$2457143.7954^{0.0017}_{0.0016}$	2457145.9418 ± 0.00033	$2457396.6382^{+0.0067}_{-0.0065}$	$2457396.5078^{+0.0022}_{-0.0023}$	2457396.5113 ± 0.0026
T_T	Time of minimum projected separation[4] (BJD$_{\rm TDB}$)	2457143.7954 ± 0.0014	$2457145.94181 \pm 0.00032$	$2457396.6382^{+0.0066}_{-0.0064}$	2457396.5078 ± 0.002	$2457396.5113^{+0.0024}_{-0.0023}$
T_0	Optimal conjunction Time[5] (BJD$_{\rm TDB}$)	2457778.0262 ± 0.0012	$2457652.79755^{+0.00027}_{-0.00028}$	$2457435.4189^{+0.0037}_{-0.0036}$	2457452.955 ± 0.0022	2457430.039 ± 0.0016
a	Semi-major axis (AU)	0.0714 ± 0.0014	$0.05174^{+0.00075}_{-0.0007}$	$0.0824^{+0.0011}_{-0.001}$	0.0738 ± 0.0021	$0.04878^{+0.00082}_{-0.00079}$
i	Inclination (Degrees)	$87.4^{+1.5}_{-0.71}$	$88.91^{+0.71}_{-0.69}$	$89.12^{+0.59}_{-0.57}$	$88.76^{+0.86}_{-1.0}$	$86.94^{+1.8}_{-0.76}$
e	Eccentricity	$0.40^{+0.30}_{-0.22}$	$0.071^{+0.11}_{-0.051}$	$0.23^{+0.42}_{-0.18}$	$0.28^{+0.37}_{-0.19}$	$0.37^{+0.31}_{-0.23}$
ω_*	Argument of Periastron (Degrees)	$20.0^{+110.0}_{-180.0}$	$-160.0^{+110.0}_{-130.0}$	$-124.0^{+100.0}_{-74.0}$	$-88.0^{+61.0}_{-63.0}$	$-210.0^{+160.0}_{-110.0}$
T_{eq}	Equilibrium temperature[6] (K)	1015.0 ± 13.0	$965.8^{+10.0}_{-9.8}$	$738.4^{+8.0}_{-7.9}$	$1148.0^{+25.0}_{-24.0}$	$1122.0^{+15.0}_{-14.0}$
$\tau_{\rm circ}$	Tidal circularization timescale (Gyr)	$61.0^{+170.0}_{-60.0}$	$153.0^{+64.0}_{-62.0}$	$11000.0^{+12000.0}_{-11000.0}$	$120.0^{+160.0}_{-120.0}$	$49.0^{+110.0}_{-48.0}$
K	RV semi-amplitude (m/s)	$3.7^{+1.8}_{-1.0}$	9.1 ± 2.3	$0.99^{+0.52}_{-0.25}$	$4.1^{+2.0}_{-1.1}$	$1.96^{+0.9}_{-0.52}$
R_P/R_*	Radius of planet in stellar radii	$0.02485^{+0.00160}_{-0.00085}$	$0.03143^{+0.00068}_{-0.00036}$	$0.01518^{+0.001}_{-0.00084}$	$0.02319^{+0.00077}_{-0.00063}$	$0.01757^{+0.0011}_{-0.00073}$
a/R_*	Semi-major axis in stellar radii	$14.76^{+0.71}_{-0.72}$	$14.11^{+0.44}_{-0.46}$	$23.16^{+0.76}_{-0.75}$	$12.64^{+0.73}_{-0.63}$	$12.03^{+0.5}_{-0.51}$
δ	$(R_P/R_*)^2$	$0.000618^{+8.3e-05}_{-4.1e-05}$	$0.000988^{+4.3e-05}_{-2.3e-05}$	$0.00023^{+3.3e-05}_{-2.5e-05}$	$0.000538^{+3.6e-05}_{-2.9e-05}$	$0.000309^{+3.9e-05}_{-2.5e-05}$
$Depth_{\rm K2}$	Flux decrement at mid transit for K2	$0.000747^{+2.9e-05}_{-3.0e-05}$	$0.001308 \pm 2.5e-05$	$0.0003 \pm 3e-05$	$0.000645^{+3.2e-05}_{-3e-05}$	$0.000365 \pm 2.1e-05$
$Depth_{\rm TESS}$	Flux decrement at mid transit for TESS	—	$0.001226^{+2.3e-05}_{-2.4e-05}$	—	$0.000623 \pm 2.9e-05$	—
τ	Ingress/egress transit duration (days)	$0.00329^{+0.0025}_{-0.00077}$	$0.0035^{+0.00071}_{-0.00055}$	$0.00216^{+0.001}_{-0.00027}$	$0.00462^{+0.0016}_{-0.00035}$	$0.00183^{+0.0013}_{-0.00044}$
T_{14}	Total transit duration (days)	$0.105^{+0.0028}_{-0.0026}$	$0.10693^{+0.001}_{-0.00088}$	$0.1293^{+0.0078}_{-0.008}$	$0.1904^{+0.005}_{-0.0046}$	$0.081^{+0.0036}_{-0.0035}$
b	Transit Impact parameter	$0.48^{+0.25}_{-0.33}$	$0.27^{+0.19}_{-0.19}$	$0.33^{+0.29}_{-0.23}$	$0.27^{+0.27}_{-0.19}$	$0.49^{+0.24}_{-0.33}$
ρ_P	Density (cgs)	$2.28^{+0.83}_{-0.54}$	$5.7^{+1.6}_{-1.5}$	$6.7^{+2.4}_{-1.3}$	$1.98^{+0.75}_{-0.46}$	$4.5^{+1.6}_{-1.1}$
$logg_P$	Surface gravity	$3.06^{+0.13}_{-0.11}$	$3.44^{+0.1}_{-0.13}$	$3.187^{+0.12}_{-0.095}$	$3.05^{+0.14}_{-0.11}$	$3.13^{+0.13}_{-0.11}$
T_S	Time of eclipse (BJD$_{\rm TDB}$)	2457140.4 ± 2.1	$2457148.3^{+0.22}_{-0.29}$	$2457401.5^{+2.0}_{-2.1}$	$2457400.0^{+1.5}_{-1.6}$	$2457398.6^{+1.1}_{-1.2}$
$T_{S,14}$	Total eclipse duration (days)	$0.109^{+0.058}_{-0.022}$	$0.105^{+0.0072}_{-0.012}$	$0.114^{+0.02}_{-0.041}$	$0.144^{+0.032}_{-0.047}$	$0.084^{+0.039}_{-0.017}$
$e\cos\omega_*$		$-0.0^{+0.50}_{-0.48}$	$-0.003^{+0.074}_{-0.095}$	$-0.0^{+0.32}_{-0.34}$	$-0.0^{+0.33}_{-0.34}$	$-0.0^{+0.43}_{-0.47}$
$e\sin\omega_*$		$0.08^{+0.2}_{-0.26}$	$-0.009^{+0.035}_{-0.082}$	$-0.073^{+0.097}_{-0.3}$	$-0.16^{+0.12}_{-0.24}$	$0.06^{+0.19}_{-0.25}$
M_P/M_*	Mass ratio	$2.84e-05^{+1.1e-05}_{-7.1e-06}$	$7.6e-05 \pm 1.9e-05$	$9.7e-06^{+3.5e-06}_{-2.1e-06}$	$3.24e-05^{+1.3e-05}_{-8.1e-06}$	$1.35e-05^{+5.1e-06}_{-3.3e-06}$
d/R_*	Separation at mid transit	$10.3^{+3.9}_{-2.7}$	$14.23^{+1.1}_{-0.91}$	$22.7^{+3.0}_{-4.1}$	13.1 ± 2.2	$9.0^{+3.0}_{-2.3}$

Notes. See Table 3 in Eastman et al. (2019) for a detailed description of all parameters. Gaussian and uniform priors are indicated as $\mathcal{G}[\text{median}, \text{width}]$ and $\mathcal{U}[\text{lower bound}, \text{upper bound}]$, respectively. Metallicity priors are adopted from TRES spectra unless otherwise indicated.
$\star$ Gaussian priors were placed on dilution in TESS only for systems with a contamination listed on EXOFOP.
[1]The metallicity of the star at birth. [2]Corresponds to static points in a star's evolutionary history. See §2 in Dotter (2016). [3]Time of conjunction is commonly reported as the "transit time". [4]Time of minimum projected separation is a more correct "transit time". [5]Optimal time of conjunction minimizes the covariance between T_C and Period. [6]Assumes no albedo and perfect redistribution.

Table 8. Median values and 68% confidence intervals.

Priors:		K2-211	K2-225	K2-226	K2-237	K2-250
π	Gaia Parallax (mas)	$\mathcal{G}[3.60379, 0.05510]$	$\mathcal{G}[2.79562, 0.04500]$	$\mathcal{G}[4.80729, 0.07400]$	$\mathcal{G}[3.29816, 0.07060]$	$\mathcal{G}[2.47572, 0.03610]$
[Fe/H]	Metallicity (dex)	$\mathcal{G}[0.115, 0.080]$	$\mathcal{G}[0.471, 0.080]$	$\mathcal{G}[-0.082, 0.080]$	$\mathcal{G}[0.357, 0.080]$	$\mathcal{G}[-0.227, 0.280]^{\dagger}$
A_V	V-band extinction (mag)	$\mathcal{U}[0, 0.08618]$	$\mathcal{U}[0, 0.11997]$	$\mathcal{U}[0, 0.21266]$	$\mathcal{U}[0, 0.58342]$	$\mathcal{U}[0, 0.11997]$
D_T^*	Dilution in *TESS*	—	—	—	$\mathcal{G}[0, 0.079682]$	—
D_K	Dilution in *K2*	—	—	—	$\mathcal{G}[0, 0.050]$	—

Parameter	Units	Values				
Stellar Parameters:						
M_*	Mass ($M_\odot$)	$0.851^{+0.039}_{-0.035}$	$1.482^{+0.11}_{-0.096}$	$0.856^{+0.042}_{-0.03}$	$1.256^{+0.055}_{-0.062}$	$0.809^{+0.044}_{-0.036}$
R_*	Radius ($R_\odot$)	$0.818^{+0.029}_{-0.027}$	$1.700^{+0.094}_{-0.087}$	$0.889^{+0.034}_{-0.032}$	$1.236^{+0.043}_{-0.036}$	$0.797^{+0.029}_{-0.027}$
L_*	Luminosity ($L_\odot$)	$0.414^{+0.017}_{-0.016}$	2.41 ± 0.11	0.558 ± 0.029	$2.01^{+0.27}_{-0.21}$	$0.359^{+0.017}_{-0.016}$
F_{Bol}	Bolometric Flux (cgs)	$1.715e-10 \pm 4.6e-12$	$6.01e-10^{+1.8e-11}_{-2e-11}$	$4.14e-10^{+1.6e-11}_{-1.9e-11}$	$7e-10^{+9.1e-11}_{-7e-11}$	$7.04e-11^{+2.6e-12}_{-2.4e-12}$
ρ_*	Density (cgs)	$2.19^{+0.25}_{-0.23}$	$0.425^{+0.047}_{-0.043}$	$1.72^{+0.22}_{-0.19}$	$0.937^{+0.073}_{-0.085}$	$2.26^{+0.24}_{-0.22}$
$\log g$	Surface gravity (cgs)	$4.543^{+0.033}_{-0.034}$	4.148 ± 0.025	$4.473^{+0.04}_{-0.034}$	$4.353^{+0.022}_{-0.029}$	$4.544^{+0.033}_{-0.032}$
T_{eff}	Effective Temperature (K)	$5117.0^{+85.0}_{-86.0}$	5520.0 ± 140.0	5288.0 ± 99.0	$6180.0^{+160.0}_{-140.0}$	5003.0 ± 94.0
[Fe/H]	Metallicity (dex)	$0.134^{+0.077}_{-0.078}$	$0.486^{+0.061}_{-0.072}$	$-0.05^{+0.068}_{-0.052}$	0.337 ± 0.076	$-0.02^{+0.24}_{-0.098}$
$[Fe/H]_0$	Initial Metallicity[1]	$0.13^{+0.078}_{-0.079}$	$0.405^{+0.057}_{-0.067}$	$-0.013^{+0.066}_{-0.06}$	$0.309^{+0.069}_{-0.07}$	$0.01^{+0.21}_{-0.1}$
Age............	Age (Gyr)	$6.5^{+4.8}_{-4.3}$	$0.0121^{+0.0039}_{-0.0032}$	$9.6^{+3.0}_{-4.7}$	$1.09^{+1.5}_{-0.78}$	$8.2^{+4.0}_{-5.0}$
EEP............	Equal Evolutionary Phase[2]	$344.0^{+24.0}_{-31.0}$	$188.0^{+4.3}_{-4.8}$	$373.0^{+28.0}_{-30.0}$	$324.0^{+28.0}_{-40.0}$	$347.0^{+19.0}_{-25.0}$
A_V	V-band extinction (mag)	$0.05^{+0.026}_{-0.032}$	$0.08^{+0.04}_{-0.046}$	$0.164^{+0.037}_{-0.07}$	$0.24^{+0.15}_{-0.14}$	$0.071^{+0.035}_{-0.045}$
σ_{SED}	SED photometry error scaling	$1.0^{+0.4}_{-0.25}$	$0.78^{+0.32}_{-0.19}$	$1.18^{+0.5}_{-0.29}$	$1.81^{+0.73}_{-0.46}$	$1.6^{+0.66}_{-0.4}$
ϖ	Parallax (mas)	3.599 ± 0.054	2.792 ± 0.045	$4.812^{+0.073}_{-0.074}$	$3.304^{+0.067}_{-0.068}$	2.478 ± 0.036
d	Distance (pc)	$277.9^{+4.2}_{-4.1}$	$358.1^{+5.8}_{-5.7}$	$207.8^{+3.3}_{-3.1}$	$302.7^{+6.3}_{-6.0}$	$403.6^{+6.0}_{-5.8}$
Planetary Parameters:						
P	Period (days)	$0.669561^{+3.1e-05}_{-3.2e-05}$	$15.8723^{+0.0021}_{-0.0019}$	3.27109 ± 0.00036	$2.18053332 \pm 5.4e-07$	4.01392 ± 0.00029
R_P	Radius (R_J)	$0.1188^{+0.0078}_{-0.0064}$	$0.322^{+0.025}_{-0.020}$	$0.1373^{+0.0092}_{-0.0077}$	$1.433^{+0.056}_{-0.049}$	$0.242^{+0.016}_{-0.012}$
M_P	Mass (M_J)	$0.0087^{+0.003}_{-0.0017}$	$0.046^{+0.017}_{-0.011}$	$0.0108^{+0.004}_{-0.0025}$	$1.366^{+0.11}_{-0.092}$	$0.0282^{+0.011}_{-0.0068}$
T_C	Time of conjunction[3] ($\mathrm{BJD_{TDB}}$)	2457393.8134 ± 0.0023	$2457587.3665^{+0.0049}_{-0.0055}$	$2457584.0262^{+0.0049}_{-0.0046}$	$2457656.463914 \pm 3.3e-05$	2457584.1282 ± 0.0031
T_T	Time of minimum projected separation[4] ($\mathrm{BJD_{TDB}}$)	2457393.8134 ± 0.0021	$2457587.3665^{+0.0046}_{-0.0051}$	$2457584.0262^{+0.0048}_{-0.0044}$	$2457656.463912 \pm 3.1e-05$	$2457584.1281^{+0.003}_{-0.0029}$
T_0	Optimal conjunction Time[5] ($\mathrm{BJD_{TDB}}$)	2457432.6479 ± 0.0013	$2457619.1111^{+0.0031}_{-0.0030}$	2457620.0082 ± 0.002	$2457706.61618 \pm 3e-05$	2457620.2535 ± 0.0015
a	Semi-major axis (AU)	$0.01419^{+0.00021}_{-0.0002}$	$0.1409^{+0.0033}_{-0.0031}$	$0.04095^{+0.00066}_{-0.00049}$	$0.03552^{+0.00051}_{-0.0006}$	$0.04606^{+0.00082}_{-0.00068}$
i	Inclination (Degrees)	$84.1^{+3.8}_{-3.0}$	$88.64^{+0.85}_{-0.60}$	$87.6^{+1.5}_{-1.1}$	$88.37^{+1.0}_{-0.88}$	$88.26^{+1.1}_{-0.94}$
e	Eccentricity	$0.19^{+0.3}_{-0.14}$	$0.23^{+0.39}_{-0.16}$	$0.22^{+0.37}_{-0.16}$	$0.03^{+0.033}_{-0.021}$	$0.21^{+0.39}_{-0.16}$
ω_*	Argument of Periastron (Degrees)	$-150.0^{+130.0}_{-110.0}$	$-160.0^{+130.0}_{-120.0}$	$-33.0^{+99.0}_{-130.0}$	$73.0^{+57.0}_{-58.0}$	$-40.0^{+92.0}_{-120.0}$
T_{eq}	Equilibrium temperature[6] (K)	$1873.0^{+22.0}_{-21.0}$	$923.0^{+13.0}_{-14.0}$	$1187.0^{+16.0}_{-17.0}$	$1759.0^{+49.0}_{-42.0}$	1003.0 ± 14.0
τ_{circ}	Tidal circularization timescale (Gyr)	$0.107^{+0.087}_{-0.095}$	$4000.0^{+4500.0}_{-3900.0}$	$53.0^{+57.0}_{-51.0}$	$0.0231^{+0.0044}_{-0.0043}$	$19.0^{+20.0}_{-19.0}$
K	RV semi-amplitude (m/s)	$2.38^{+0.89}_{-0.5}$	$3.13^{+1.5}_{-0.83}$	$1.79^{+0.81}_{-0.46}$	$184.0^{+14.0}_{-11.0}$	$4.5^{+2.2}_{-1.2}$
R_P/R_*	Radius of planet in stellar radii	$0.01489^{+0.00079}_{-0.00059}$	$0.01942^{+0.00091}_{-0.00064}$	$0.01586^{+0.00082}_{-0.00068}$	$0.119^{+0.0024}_{-0.0023}$	$0.0311^{+0.0016}_{-0.001}$
a/R_*	Semi-major axis in stellar radii	3.73 ± 0.13	$17.82^{+0.64}_{-0.62}$	$9.91^{+0.41}_{-0.37}$	$6.18^{+0.16}_{-0.19}$	$12.44^{+0.43}_{-0.42}$
δ	$(R_P/R_*)^2$	$0.000222^{+2.4e-05}_{-1.7e-05}$	$0.000377^{+3.6e-05}_{-2.4e-05}$	$0.000252^{+2.7e-05}_{-2.1e-05}$	$0.01416^{+0.00058}_{-0.00053}$	$0.00097^{+0.0001}_{-6.2e-05}$
$Depth_{K2}$	Flux decrement at mid transit for *K2*	$0.000287 \pm 1.9e-05$	$0.000465 \pm 2.6e-05$	$0.000314 \pm 2.3e-05$	$0.0169^{+0.00072}_{-0.00067}$	$0.001284^{+7e-05}_{-7.2e-05}$
$Depth_{TESS}$	Flux decrement at mid transit for *TESS*	—	—	—	$0.01624^{+0.00072}_{-0.00068}$	—
τ	Ingress/egress transit duration (days)	$0.00092^{+0.00037}_{-0.00012}$	$0.00572^{+0.0026}_{-0.00082}$	$0.00176^{+0.00076}_{-0.00025}$	$0.01347^{+0.00054}_{-0.00041}$	$0.00336^{+0.0014}_{-0.00041}$
T_{14}	Total transit duration (days)	$0.0538^{+0.003}_{-0.0031}$	$0.258^{+0.0073}_{-0.0064}$	$0.0968^{+0.0046}_{-0.0047}$	$0.12197^{+0.00038}_{-0.00034}$	0.0986 ± 0.0037
b	Transit Impact parameter	0.36 ± 0.24	$0.38^{+0.24}_{-0.25}$	$0.38^{+0.24}_{-0.25}$	$0.171^{+0.091}_{-0.11}$	$0.35^{+0.25}_{-0.23}$
ρ_P	Density (cgs)	$6.4^{+2.2}_{-1.3}$	$1.67^{+0.61}_{-0.4}$	$5.1^{+1.9}_{-1.2}$	$0.577^{+0.069}_{-0.064}$	$2.41^{+0.88}_{-0.56}$
$logg_P$	Surface gravity	$3.182^{+0.12}_{-0.09}$	$3.03^{+0.13}_{-0.11}$	$3.15^{+0.13}_{-0.1}$	3.218 ± 0.039	$3.07^{+0.13}_{-0.11}$
T_S	Time of eclipse ($\mathrm{BJD_{TDB}}$)	$2457393.48^{+0.11}_{-0.12}$	$2457595.3^{+3.4}_{-3.5}$	2457582.39 ± 0.68	$2457655.38^{+0.031}_{-0.021}$	2457586.13 ± 0.81
$T_{S,14}$	Total eclipse duration (days)	$0.0517^{+0.079}_{-0.011}$	$0.249^{+0.046}_{-0.081}$	$0.092^{+0.016}_{-0.027}$	$0.1266^{+0.0087}_{-0.0049}$	$0.092^{+0.014}_{-0.029}$
$e \cos \omega_*$	....	$-0.0^{+0.26}_{-0.27}$	$0.0^{+0.34}_{-0.35}$	$0.0^{+0.32}_{-0.33}$	$0.005^{+0.023}_{-0.015}$	$-0.0^{+0.31}_{-0.26}$
$e \sin \omega_*$	....	$-0.024^{+0.083}_{-0.18}$	$-0.023^{+0.097}_{-0.21}$	$-0.033^{+0.094}_{-0.25}$	$0.019^{+0.035}_{-0.02}$	$-0.038^{+0.083}_{-0.26}$
M_P/M_*	Mass ratio	$9.8e-06^{+3.4e-06}_{-1.9e-06}$	$2.94e-05^{+1.1e-05}_{-7e-06}$	$1.2e-05^{+4.5e-06}_{-2.8e-06}$	$0.001041^{+8.2e-05}_{-6.4e-05}$	$3.32e-05^{+1.3e-05}_{-8e-06}$
d/R_*	Separation at mid transit	$3.62^{+0.46}_{-0.52}$	$16.6^{+2.5}_{-3.1}$	$9.4^{+1.3}_{-1.7}$	$6.06^{+0.27}_{-0.39}$	$12.0^{+1.5}_{-2.0}$

Notes. See Table 3 in Eastman et al. (2019) for a detailed description of all parameters. Gaussian and uniform priors are indicated as $\mathcal{G}$[median, width] and $\mathcal{U}$[lower bound, upper bound], respectively. Metallicity priors are adopted from TRES spectra unless otherwise indicated. * Gaussian priors were placed on dilution in *TESS* only for systems with a contamination listed on EXOFOP. † From Huber et al. (2016). [1]The metallicity of the star at birth. [2]Corresponds to static points in a star's evolutionary history. See §2 in Dotter (2016). [3]Time of conjunction is commonly reported as the "transit time". [4]Time of minimum projected separation is a more correct "transit time". [5]Optimal time of conjunction minimizes the covariance between T_C and Period. [6]Assumes no albedo and perfect redistribution.

Table 9. Median values and 68% confidence intervals.

Priors:		K2-260	K2-261†	K2-261†	K2-265	K2-277	K2-321′
π	Gaia Parallax (mas)	$\mathcal{G}[1.49761,0.04250]$	$\mathcal{G}[4.68526,0.04270]$		$\mathcal{G}[7.18885,0.05050]$	$\mathcal{G}[8.84150,0.06199]$	—
[Fe/H]	Metallicity (dex)	$\mathcal{G}[0.386,0.080]$	$\mathcal{G}[0.382,0.080]$		$\mathcal{G}[0.08,0.08]$	$\mathcal{G}[0.064,0.080]$	—
A_V	V-band extinction (mag)	$\mathcal{U}[0,0.82243]$	$\mathcal{U}[0,0.12679]$		$\mathcal{U}[0,0.11408]$	$\mathcal{U}[0,0.19933]$	—
D_T^*	Dilution in TESS	$\mathcal{G}[0,0.036733]$	$\mathcal{G}[0,0.0021478]$		—	$\mathcal{G}[0,0.0020849]$	$\mathcal{G}[0,0.0035631]$

Parameter	Units	Values					
Stellar Parameters:							
M_*	Mass ($M_\odot$)	$1.637^{+0.065}_{-0.069}$	$1.107^{+0.042}_{-0.047}$	1.264 ± 0.041	$0.901^{+0.051}_{-0.042}$	$0.974^{+0.053}_{-0.058}$	0.578 ± 0.03
R_*	Radius ($R_\odot$)	$1.755^{+0.061}_{-0.078}$	$1.663^{+0.071}_{-0.068}$	$1.609^{+0.061}_{-0.057}$	$0.92^{+0.034}_{-0.032}$	$0.973^{+0.038}_{-0.035}$	0.595 ± 0.031
L_*	Luminosity ($L_\odot$)	$6.14^{+0.48}_{-0.52}$	$2.259^{+0.087}_{-0.083}$	$2.275^{+0.085}_{-0.084}$	0.657 ± 0.024	$0.89^{+0.048}_{-0.044}$	$0.063^{+0.042}_{-0.028}$
F_{Bol}	Bolometric Flux (cgs)	$4.36e-10^{+1.9e-11}_{-3e-11}$	$1.588e-09^{+5.5e-11}_{-5.1e-11}$	$1.599e-09^{+5.2e-11}_{-5.3e-11}$	$1.087e-09\pm3.7e-11$	$2.22e-09^{+1.2e-10}_{-1.1e-10}$	—
ρ_*	Density (cgs)	$0.424^{+0.067}_{-0.039}$	$0.339^{+0.046}_{-0.042}$	$0.427^{+0.046}_{-0.041}$	$1.63^{+0.22}_{-0.19}$	1.5 ± 0.2	$3.86^{+0.7}_{-0.57}$
$\log g$	Surface gravity (cgs)	$4.161^{+0.044}_{-0.03}$	$4.040^{+0.038}_{-0.041}$	$4.126^{+0.030}_{-0.028}$	$4.465^{+0.042}_{-0.039}$	$4.452^{+0.041}_{-0.049}$	$4.65^{+0.051}_{-0.049}$
$T_{\rm eff}$	Effective Temperature (K)	$6860.0^{+150.0}_{-160.0}$	5490 ± 110	5587 ± 100	5420.0 ± 100.0	5680 ± 120.0	$3750.0^{+510.0}_{-520.0}$
[Fe/H]	Metallicity (dex)	$0.334^{+0.052}_{-0.061}$	$0.372^{+0.069}_{-0.072}$	$0.401^{+0.064}_{-0.070}$	$0.033^{+0.099}_{-0.1}$	$0.078^{+0.072}_{-0.065}$	0.148 ± 0.062
$[{\rm Fe/H}]_0$	Initial Metallicity[1]	$0.44^{+0.04}_{-0.056}$	$0.368^{+0.064}_{-0.068}$	$0.396^{+0.057}_{-0.064}$	$0.051^{+0.096}_{-0.091}$	$0.084^{+0.072}_{-0.069}$	—
Age	Age (Gyr)	$0.65^{+0.43}_{-0.37}$	$8.8^{+1.7}_{-1.2}$	$4.78^{+0.72}_{-0.78}$	$7.8^{+4.0}_{-4.6}$	$4.9^{+4.8}_{-3.4}$	—
EEP	Equal Evolutionary Phase[2]	$327.0^{+13.0}_{-26.0}$	$455.4^{+4.6}_{-5.7}$	$413.3^{+9.4}_{-15}$	$366.0^{+29.0}_{-32.0}$	$350.0^{+45.0}_{-32.0}$	—
A_V	V-band extinction (mag)	$0.766^{+0.041}_{-0.079}$	$0.060^{+0.045}_{-0.041}$	$0.074^{+0.037}_{-0.047}$	$0.071^{+0.031}_{-0.042}$	$0.099^{+0.065}_{-0.066}$	—
σ_{SED}	SED photometry error scaling	$0.56^{+0.24}_{-0.14}$	$0.81^{+0.32}_{-0.20}$	$0.82^{+0.33}_{-0.20}$	$0.95^{+0.41}_{-0.26}$	$0.75^{+0.27}_{-0.17}$	—
ϖ	Parallax (mas)	1.486 ± 0.041	4.688 ± 0.043	4.687 ± 0.042	$7.19^{+0.051}_{-0.05}$	8.838 ± 0.062	—
d	Distance (pc)	$672.0^{+19.0}_{-18.0}$	$213.3^{+2.0}_{-1.9}$	213.3 ± 1.9	$139.08^{+0.98}_{-0.97}$	$113.14^{+0.8}_{-0.78}$	—
Planetary Parameters:							
P	Period (days)	$2.62669762\pm6.6e-07$	$11.6334681\pm4.4e-06$	$11.6334681\pm4.4e-06$	$2.36902^{+5.8e-05}_{-5.9e-05}$	$6.326768^{+1.5e-05}_{-1.2e-05}$	$2.2979749^{+1.7e-06}_{-1.9e-06}$
R_P	Radius (R_J)	$1.643^{+0.058}_{-0.073}$	$0.856^{+0.038}_{-0.036}$	$0.827^{+0.033}_{-0.057}$	$0.1524^{+0.01}_{-0.0077}$	$0.195^{+0.018}_{-0.011}$	$0.183^{+0.015}_{-0.012}$
M_P	Mass (M_J)	$1.72^{+0.34}_{-0.35}$	$0.194^{+0.024}_{-0.023}$	$0.217^{+0.025}_{-0.024}$	$0.0231^{+0.0045}_{-0.0044}$	$0.0197^{+0.0076}_{-0.0069}$	$0.0178^{+0.0076}_{-0.0069}$
T_C	Time of conjunction[3] (BJD$_{\rm TDB}$)	$2457820.737343\pm6.3e-05$	$2457906.84110^{+0.00028}_{-0.00033}$	$2457906.84108^{+0.00026}_{-0.00029}$	$2456981.6455^{+0.0011}_{-0.001}$	2457221.2291 ± 0.0011	$2457909.17213^{+0.00069}_{-0.00071}$
T_T	Time of minimum projected separation[4] (BJD$_{\rm TDB}$)	$2457820.737341\pm6e-05$	2457906.84130 ± 0.00022	2457906.84124 ± 0.00022	$2456981.64531^{+0.00099}_{-0.00098}$	$2457221.22914^{+0.00064}_{-0.00063}$	2457909.17213 ± 0.00051
T_0	Optimal conjunction Time[5] (BJD$_{\rm TDB}$)	$2457894.284876^{+6e-05}_{-5.9e-05}$	$2458151.14394^{+0.00027}_{-0.00032}$	$2458151.14392^{+0.00024}_{-0.00027}$	$2457017.18078^{+0.00055}_{-0.00054}$	2457303.4771 ± 0.001	$2458141.26759^{+0.00064}_{-0.00068}$
a	Semi-major axis (AU)	$0.04392^{+0.00057}_{-0.00063}$	$0.1040^{+0.0013}_{-0.0015}$	0.1086 ± 0.0012	$0.03359^{+0.00062}_{-0.00053}$	$0.0664^{+0.0012}_{-0.0013}$	$0.02839^{+0.00048}_{-0.0005}$
i	Inclination (Degrees)	$89.18^{+0.58}_{-0.83}$	$88.24^{+1.0}_{-0.67}$	$88.58^{+0.85}_{-0.57}$	$87.01^{+1.8}_{-1.0}$	$86.83^{+1.6}_{-0.96}$	$86.1^{+2.5}_{-1.1}$
e	Eccentricity	$0.053^{+0.051}_{-0.036}$	$0.331^{+0.063}_{-0.066}$	$0.274^{+0.065}_{-0.061}$	$0.16^{+0.16}_{-0.11}$	$0.52^{+0.24}_{-0.26}$	$0.44^{+0.26}_{-0.23}$
ω_*	Argument of Periastron (Degrees)	$-72.0^{+74.0}_{-79.0}$	137^{+13}_{-16}	145^{+13}_{-15}	$-57.0^{+52.0}_{-27.0}$	$46.0^{+96.0}_{-120.0}$	$45.0^{+96.0}_{-140.0}$
T_{eq}	Equilibrium temperature[6] (K)	$2090.0^{+35.0}_{-39.0}$	1058 ± 11	$1036\pm10.$	1366.0 ± 17.0	1049 ± 15.0	830.0 ± 110.0
$\tau_{\rm circ}$	Tidal circularization timescale (Gyr)	$0.0381^{+0.011}_{-0.0099}$	$15.8^{+12}_{-7.3}$	33^{+19}_{-14}	$23.0^{+14.0}_{-15.0}$	$31.0^{+210.0}_{-31.0}$	$0.76^{+2.8}_{-0.74}$
K	RV semi-amplitude (m/s)	$182.0^{+36.0}_{-37.0}$	$17.3^{+2.1}_{-2.5}$	$17.4^{+1.9}_{-2.3}$	$3.87^{+1.0}_{-0.75}$	$2.73^{+1.3}_{-0.75}$	$4.6^{+2.3}_{-1.3}$
R_P/R_*	Radius of planet in stellar radii	$0.09617^{+0.00024}_{-0.00019}$	$0.05279^{+0.00079}_{-0.00054}$	$0.05274^{+0.00076}_{-0.00049}$	$0.01695^{+0.00095}_{-0.00045}$	$0.02045^{+0.0019}_{-0.00074}$	$0.0315^{+0.0021}_{-0.0013}$
a/R_*	Semi-major axis in stellar radii	$5.37^{+0.27}_{-0.17}$	13.43 ± 0.58	$14.51^{+0.51}_{-0.47}$	$7.86^{+0.33}_{-0.31}$	$14.68^{+0.64}_{-0.7}$	$10.25^{+0.58}_{-0.53}$
δ	$(R_P/R_*)^2$	$0.00925^{+4.5e-05}_{-3.7e-05}$	$0.002787^{+8.5e-05}_{-5.6e-05}$	$0.002781^{+4.5e-05}_{-5.2e-05}$	$0.000287^{+3.3e-05}_{-1.5e-05}$	$0.000418^{+7.9e-05}_{-3e-05}$	$0.000992^{+0.00014}_{-7.8e-05}$
$Depth_{\rm K2}$	Flux decrement at mid transit for K2	0.01042 ± 0.00011	$0.003571^{+6.7e-05}_{-6.4e-05}$	$0.003553^{+6.5e-05}_{-6.2e-05}$	$0.00035\pm1.1e-05$	$0.000482^{+1.7e-05}_{-1.9e-05}$	$0.001167^{+8.6e-05}_{-6.5e-05}$
$Depth_{\rm TESS}$	Flux decrement at mid transit for TESS	0.01007 ± 0.00014	$0.003353\pm5.2e-05$	$0.003332\pm5.0e-05$	—	$0.000469^{+1.6e-05}_{-1.7e-05}$	$0.00114^{+8.7e-05}_{-9.2e-05}$
τ	Ingress/egress transit duration (days)	$0.015594^{+0.00033}_{-9.5e-05}$	$0.0117^{+0.0016}_{-0.0010}$	$0.01163^{+0.0016}_{-0.00092}$	$0.00198^{+0.0013}_{-0.00037}$	$0.00227^{+0.003}_{-0.00065}$	$0.00183^{+0.0017}_{-0.00041}$
T_{14}	Total transit duration (days)	$0.17496^{+0.00035}_{-0.00032}$	$0.2138^{+0.0015}_{-0.0011}$	$0.2137^{+0.0014}_{-0.0011}$	$0.0962^{+0.0018}_{-0.0016}$	$0.0819^{+0.0028}_{-0.0023}$	0.0478 ± 0.0017
b	Transit Impact parameter	$0.08^{+0.08}_{-0.056}$	$0.30^{+0.14}_{-0.18}$	$0.29^{+0.14}_{-0.18}$	$0.44^{+0.26}_{-0.28}$	$0.53^{+0.28}_{-0.36}$	$0.47^{+0.29}_{-0.33}$
ρ_P	Density (cgs)	$0.48^{+0.12}_{-0.11}$	$0.381^{+0.078}_{-0.072}$	$0.473^{+0.082}_{-0.079}$	$7.9^{+2.1}_{-1.9}$	$3.18^{+1.2}_{-0.76}$	$3.55^{+1.4}_{-0.88}$
$logg_P$	Surface gravity	$3.199^{+0.085}_{-0.1}$	$2.815^{+0.066}_{-0.080}$	$2.895^{+0.058}_{-0.070}$	$3.385^{+0.09}_{-0.1}$	$3.1^{+0.13}_{-0.11}$	$3.11^{+0.14}_{-0.12}$
T_S	Time of eclipse (BJD$_{\rm TDB}$)	$2457819.432^{+0.082}_{-0.063}$	$2457906.91^{+0.61}_{-0.62}$	$2457911.04^{+0.51}_{-0.55}$	2456980.58 ± 0.1	2457221.1 ± 2.2	$2457908.02^{+0.7}_{-0.72}$
$T_{S,14}$	Total eclipse duration (days)	$0.167^{+0.011}_{-0.016}$	$0.310^{+0.053}_{-0.043}$	$0.281^{+0.035}_{-0.031}$	$0.082^{+0.013}_{-0.016}$	$0.082^{+0.062}_{-0.042}$	$0.05^{+0.034}_{-0.011}$
$e\cos\omega_*$		$0.005^{+0.049}_{-0.037}$	$-0.233^{+0.048}_{-0.082}$	$-0.218^{+0.070}_{-0.077}$	$0.075^{+0.067}_{-0.065}$	$0.0^{+0.56}_{-0.54}$	$-0.0^{+0.49}_{-0.5}$
$e\sin\omega_*$		$-0.024^{+0.032}_{-0.051}$	$0.220^{+0.059}_{-0.064}$	$0.155^{+0.050}_{-0.057}$	$-0.093^{+0.093}_{-0.21}$	$0.15^{+0.26}_{-0.33}$	$0.14^{+0.2}_{-0.24}$
M_P/M_*	Mass ratio	0.001 ± 0.0002	$0.000168^{+2.0e-05}_{-2.4e-05}$	$0.000164^{+1.8e-05}_{-2.2e-05}$	$2.44e-05\pm4.7e-06$	$1.94e-05^{+7.7e-06}_{-4.9e-06}$	$2.94e-05^{+1.3e-05}_{-7.6e-06}$
d/R_*	Separation at mid transit	$5.48^{+0.56}_{-0.33}$	$9.8^{+1.2}_{-1.1}$	$11.6^{+1.2}_{-1.0}$	$8.58^{+1.6}_{-0.9}$	$8.4^{+5.4}_{-2.4}$	$6.6^{+2.9}_{-1.8}$

Notes. See Table 3 in Eastman et al. (2019) for a detailed description of all parameters. Gaussian and uniform priors are indicated as $\mathcal{G}[\text{median},\text{width}]$ and $\mathcal{U}[\text{lower bound},\text{upper bound}]$, respectively. Metallicity priors are adopted from TRES spectra unless otherwise indicated. * Gaussian priors were placed on dilution in TESS only for systems with a contamination listed on EXOFOP. $'$ The stellar parameters from the global fit are not considered reliable as the SED was not included within this fit. † The PDFs for K2-261 showed bimodality of the host star's mass and age (See §4.1.3). The two solutions are shown here, but we adopt the low mass solutions for figures as it has a higher probability.

[1] The metallicity of the star at birth. [2] Corresponds to static points in a star's evolutionary history. See §2 in Dotter (2016). [3] Time of conjunction is commonly reported as the "transit time". [4] Time of minimum projected separation is a more correct "transit time". [5] Optimal time of conjunction minimizes the covariance between T_C and Period. [6] Assumes no albedo and perfect redistribution.

Table 10. Median values and 68% confidence intervals for the global models for *K2* fits only.

System	*K2* Campaign	Wavelength Parameters		Transit Parameters	
		$u_1^{\dagger}$	$u_2^{\ddagger}$	$\sigma^{2\star}$	F_0^{*}
K2-7	C1	0.394 ± 0.054	0.261 ± 0.051	$-0.0000000095^{+0.0000000051}_{-0.0000000045}$	$0.999998^{+0.000018}_{-0.000019}$
K2-54	C3	0.44 ± 0.17	$0.24^{+0.17}_{-0.18}$	$0.0000000087^{+0.000000011}_{-0.0000000097}$	1.000000 ± 0.000029
K2-57	C3	0.677 ± 0.054	$0.076^{+0.053}_{-0.054}$	$0.000000001^{+0.000000013}_{-0.000000010}$	1.000021 ± 0.000031
K2-147	C7	$0.28^{+0.17}_{-0.15}$	0.35 ± 0.18	$0.0000000111^{+0.0000000033}_{-0.0000000030}$	$1.0000077^{+0.000010}_{-0.0000100}$
K2-181	C5	$0.480^{+0.042}_{-0.041}$	0.217 ± 0.038	$0.0000000110^{+0.0000000027}_{-0.0000000024}$	$0.999996^{+0.000012}_{-0.000011}$
	C18	$0.480^{+0.042}_{-0.041}$	0.217 ± 0.038	$0.0000000020^{+0.0000000025}_{-0.0000000022}$	1.000010 ± 0.000012
K2-203	C8	0.561 ± 0.054	0.158 ± 0.052	$0.0000000038^{+0.0000000017}_{-0.0000000015}$	0.999997 ± 0.000010
K2-204	C8	$0.372^{+0.055}_{-0.054}$	$0.253^{+0.051}_{-0.052}$	$0.0000000095^{+0.0000000033}_{-0.0000000030}$	0.999995 ± 0.000012
K2-208	C8	0.447 ± 0.055	$0.237^{+0.051}_{-0.053}$	$0.00000000067^{+0.00000000100}_{-0.00000000091}$	$0.9999965^{+0.0000069}_{-0.0000070}$
K2-211	C8	0.548 ± 0.055	0.166 ± 0.052	$0.0000000056 \pm 0.0000000012$	$1.0000020^{+0.0000057}_{-0.0000056}$
K2-225	C10	0.468 ± 0.058	0.210 ± 0.054	$0.0000000029^{+0.0000000014}_{-0.0000000012}$	1.000031 ± 0.000011
K2-226	C10	$0.492^{+0.056}_{-0.055}$	0.203 ± 0.053	$0.0000000019^{+0.0000000013}_{-0.0000000012}$	1.0000034 ± 0.0000081
K2-250	C10	0.576 ± 0.058	0.157 ± 0.054	$0.0000000115^{+0.0000000063}_{-0.0000000057}$	1.000006 ± 0.000015
K2-265	C3	0.466 ± 0.054	0.215 ± 0.052	$-0.00000000033^{+0.00000000015}_{-0.00000000014}$	0.9999979 ± 0.0000025

Notes. [†] Linear limb-darkening coefficient. [‡] Quadratic limb-darkening coefficient. [⋆] Added variance. [*] Baseline flux.

Table 11. Median values and 68% confidence intervals for the global models for *K2* and *TESS* fits.

System	Campaign/Sector	Wavelength Parameters $u_1^{\dagger}$	$u_2^{\ddagger}$	Transit Parameters $\sigma^{2\star}$	F_0^*	Dilution A_D
K2-77	*K2* C4	0.506 ± 0.059	0.151 ± 0.055	$0.0000000036^{+0.0000000016}_{-0.0000000013}$	1.000009 ± 0.000010	
	TESS S5	$0.411^{+0.034}_{-0.035}$	0.218 ± 0.029	$0.000000178^{+0.000000050}_{-0.000000049}$	0.999994 ± 0.000016	0.00000 ± 0.00024
	TESS S42			$0.000000028^{+0.00000059}_{-0.00000058}$	1.000003 ± 0.000019	
	TESS S43			$0.000000118^{+0.000000054}_{-0.000000053}$	1.000007 ± 0.000017	
	TESS S44			$-0.000000085^{+0.000000050}_{-0.000000049}$	1.000012 ± 0.000017	
K2-97	*K2* C5	$0.652^{+0.040}_{-0.041}$	0.098 ± 0.039	$0.0000000070^{+0.0000000031}_{-0.0000000028}$	0.999995 ± 0.000011	
	K2 C18			$0.0000000149^{+0.0000000048}_{-0.0000000043}$	0.999996 ± 0.000014	
	TESS S7	0.488 ± 0.029	0.181 ± 0.026	$0.000000159^{+0.000000070}_{-0.000000069}$	1.000000 ± 0.000020	-0.27 ± 0.12
	TESS S44			$0.000000244^{+0.000000083}_{-0.000000082}$	1.000001 ± 0.000022	
	TESS S45			$-0.000000001^{+0.000000084}_{-0.000000083}$	0.999988 ± 0.000022	
	TESS S46			$0.000000148^{+0.000000072}_{-0.000000070}$	1.000008 ± 0.000020	
K2-98	*K2* C5	$0.325^{+0.037}_{-0.036}$	0.305 ± 0.036	$0.0000000017^{+0.0000000012}_{-0.0000000010}$	$1.0000098^{+0.0000075}_{-0.0000074}$	
	K2 C18			$0.0000000044^{+0.0000000020}_{-0.0000000018}$	0.999991 ± 0.000010	
	TESS S7	$0.235^{+0.028}_{-0.027}$	0.304 ± 0.023	$-0.00000003^{+0.00000031}_{-0.00000029}$	1.000088 ± 0.000085	-0.0000 ± 0.0019
	TESS S34			$0.00000057^{+0.00000045}_{-0.00000042}$	1.00015 ± 0.00010	
	TESS S44			$0.00000017^{+0.00000033}_{-0.00000031}$	$0.999879^{+0.000088}_{-0.000087}$	
	TESS S45			$0.00000045^{+0.00000033}_{-0.00000031}$	$0.999931^{+0.000086}_{-0.000085}$	
	TESS S46			$0.00000059^{+0.00000030}_{-0.00000028}$	1.000249 ± 0.000095	
K2-114	*K2* C5	$0.611^{+0.025}_{-0.026}$	$0.106^{+0.036}_{-0.035}$	$0.000000012^{+0.000000018}_{-0.000000016}$	1.000034 ± 0.000032	
	K2 C18			$0.00000082 \pm 0.00000013$	$0.999745^{+0.000044}_{-0.000043}$	
	TESS S7	0.473 ± 0.026	$0.189^{+0.026}_{-0.025}$	$-0.0000060^{+0.0000062}_{-0.0000058}$	$0.99980^{+0.00042}_{-0.00043}$	$-0.027^{+0.034}_{-0.035}$
	TESS S44			$-0.0000000^{+0.0000076}_{-0.0000071}$	0.99925 ± 0.00047	
	TESS S45			$0.0000153^{+0.0000093}_{-0.0000088}$	0.99999 ± 0.00051	
	TESS S46			$-0.0000077^{+0.0000068}_{-0.0000064}$	0.99941 ± 0.00044	
K2-115	*K2* C5	0.365 ± 0.035	0.278 ± 0.036	$0.0000000117^{+0.0000000070}_{-0.0000000058}$	0.999993 ± 0.000023	
	K2 C18			$0.000000028^{+0.000000016}_{-0.000000013}$	0.999966 ± 0.000037	
	TESS S7	0.274 ± 0.032	0.285 ± 0.026	$0.0000013^{+0.0000015}_{-0.0000014}$	1.00008 ± 0.00018	-0.000000 ± 0.000014
	TESS S34			$0.0000033^{+0.0000033}_{-0.0000030}$	0.99972 ± 0.00034	
	TESS S45			$-0.0000020^{+0.0000016}_{-0.0000015}$	$0.99999^{+0.00020}_{-0.00021}$	
	TESS S46			$-0.0000024^{+0.0000020}_{-0.0000018}$	0.99930 ± 0.00027	
K2-167	*K2* C3	0.320 ± 0.050	0.314 ± 0.050	$-0.00000000008^{+0.0000000022}_{-0.0000000018}$	0.9999986 ± 0.0000041	
	TESS S2	0.224 ± 0.031	0.300 ± 0.029	$0.0000000005^{+0.0000000047}_{-0.0000000044}$	0.999982 ± 0.000011	0.000000 ± 0.000027
	TESS S28			$-0.0000015010^{+0.000000039}_{-0.000000019}$	$1.000031^{+0.000038}_{-0.000032}$	
	TESS S42			$0.000000017^{+0.000000012}_{-0.000000010}$	1.000000 ± 0.000021	
K2-180	*K2* C5	$0.416^{+0.042}_{-0.041}$	$0.253^{+0.038}_{-0.039}$	$0.0000000016^{+0.0000000029}_{-0.0000000025}$	0.999998 ± 0.000013	
	K2 C18			$0.0000000196^{+0.0000000070}_{-0.0000000059}$	1.000017 ± 0.000021	
	TESS S7	$0.323^{+0.030}_{-0.029}$	$0.268^{+0.24}_{-0.025}$	$0.00000007^{+0.00000031}_{-0.00000022}$	0.99953 ± 0.00019	-0.012 ± 0.039
	TESS S34			$0.0000011^{+0.0000011}_{-0.0000010}$	1.00028 ± 0.00016	
	TESS S44			$0.00000045^{+0.00000011}_{-0.000000097}$	0.99981 ± 0.00016	
	TESS S45			$0.00000168^{+0.00000081}_{-0.00000077}$	0.99983 ± 0.00014	
	TESS S46			$-0.00000158^{+0.00000069}_{-0.00000064}$	0.99985 ± 0.00013	
K2-182	*K2* C5	0.528 ± 0.035	0.167 ± 0.038	$0.00000000059^{+0.0000000059}_{-0.0000000053}$	$0.9999964^{+0.0000051}_{-0.0000050}$	
	K2 C18			$0.00000000107^{+0.0000000095}_{-0.0000000085}$	1.0000071 ± 0.0000067	
	TESS S7	0.416 ± 0.027	0.219 ± 0.024	$-0.000000031^{+0.000000039}_{-0.000000031}$	1.000089 ± 0.000052	-0.00000 ± 0.00029
	TESS S34			$0.00000022^{+0.00000019}_{-0.00000018}$	$1.000116^{+0.000059}_{-0.000058}$	
	TESS S44			$0.00000002^{+0.00000019}_{-0.00000018}$	0.999984 ± 0.000065	
	TESS S45			$0.00000027^{+0.00000020}_{-0.00000019}$	1.000113 ± 0.000067	
	TESS S46			$0.00000009^{+0.00000018}_{-0.00000017}$	0.999995 ± 0.000063	
K2-237	*K2* C11-1	$0.337^{+0.014}_{-0.015}$	0.250 ± 0.034	$0.0000000056^{+0.0000000021}_{-0.0000000018}$	$1.0000000^{+0.0000096}_{-0.0000097}$	$0.006^{+0.039}_{-0.040}$
	K2 C11-2			$0.00000000385^{+0.0000000010}_{-0.00000000092}$	0.9999947 ± 0.0000062	
	TESS S12	0.266 ± 0.033	0.305 ± 0.035	0.0000217 ± 0.0000013	1.00025 ± 0.00015	$-0.050^{+0.042}_{-0.043}$
	TESS S39			$0.0001052^{+0.0000031}_{-0.0000030}$	1.00057 ± 0.00014	
K2-260	*K2* C13	0.228 ± 0.017	0.323 ± 0.037	$0.0000000061^{+0.0000000012}_{-0.0000000011}$	$0.9999861^{+0.0000058}_{-0.0000059}$	
	TESS S5	0.164 ± 0.026	0.321 ± 0.028	$-0.00000027^{+0.00000012}_{-0.00000011}$	$1.000021^{+0.000072}_{-0.000073}$	0.027 ± 0.011
	TESS S32			$0.00000086^{+0.00000051}_{-0.00000049}$	$1.000154^{+0.000082}_{-0.000083}$	
	TESS S43			$-0.00000027^{+0.00000036}_{-0.00000035}$	$0.999843^{+0.000072}_{-0.000073}$	
K2-261	*K2* C14	0.474 ± 0.031	0.208 ± 0.046	$0.0000000157^{+0.00000000065}_{-0.00000000057}$	0.9999974 ± 0.0000059	
	TESS S9	0.363 ± 0.027	0.257 ± 0.027	$0.000000106^{+0.000000050}_{-0.000000047}$	1.000048 ± 0.000034	0.0002 ± 0.0021
	TESS S35			$0.00000388^{+0.00000018}_{-0.00000017}$	1.000253 ± 0.000041	
	TESS S45			$0.00000017^{+0.000000054}_{-0.000000051}$	0.999950 ± 0.000035	
	TESS S46			$0.000000004^{+0.000000050}_{-0.000000046}$	1.000102 ± 0.000034	
K2-277	*K2* C6	$0.419^{+0.055}_{-0.054}$	0.250 ± 0.052	$0.00000000110^{+0.00000000033}_{-0.00000000028}$	$0.9999913^{+0.0000046}_{-0.0000045}$	
	TESS S10	0.322 ± 0.040	$0.270^{+0.036}_{-0.037}$	$-0.000000010^{+0.000000044}_{-0.000000041}$	1.000020 ± 0.000034	-0.0000 ± 0.0021
	TESS S37			$0.000000024^{+0.000000012}_{-0.000000011}$	1.0000220 ± 0.0000080	
K2-321	*K2* C14	$0.41^{+0.16}_{-0.17}$	$0.33^{+0.17}_{-0.18}$	$0.0000000045^{+0.0000000025}_{-0.0000000023}$	1.000003 ± 0.000010	
	TESS S8	0.38 ± 0.17	$0.30^{+0.17}_{-0.18}$	$0.00000023 \pm 0.00000012$	1.000003 ± 0.000028	0.0001 ± 0.0037
	TESS S35			$-0.000000009^{+0.000000044}_{-0.000000042}$	0.999998 ± 0.000025	
	TESS S45			$0.000000078^{+0.000000099}_{-0.000000096}$	1.000015 ± 0.000024	
	TESS S46			$-0.000000001^{+0.00000011}_{-0.00000010}$	$1.000000^{+0.000024}_{-0.000025}$	

Notes. [†] Linear limb-darkening coefficient. [‡] Quadratic limb-darkening coefficient. [⋆] Added variance. [*] Baseline flux.

Table 12. Median values and 68% confidence intervals for the radial velocity parameters.

K2-97				
Telescope Parameters:		HIRES	LEVY	
$\gamma_{\rm rel}$.	Relative RV Offset (m/s)	-5.2 ± 1.6	12^{+16}_{-19}	
σ_J ..	RV Jitter (m/s)	$5.8^{+1.6}_{-1.2}$	26^{+35}_{-27}	
σ_J^2 ..	RV Jitter Variance	33^{+21}_{-12}	720^{+3100}_{-900}	
K2-98				
Telescope Parameters:		FIES	HARPS	HARPS-N
$\gamma_{\rm rel}$.	Relative RV Offset (m/s)	$76612.0^{+4.5}_{-4.3}$	76747.7 ± 3.3	76740.8 ± 4.0
σ_J ..	RV Jitter (m/s)	$7.03^{+0.94}_{-2.2}$	$1.55^{+0.12}_{-0.43}$	$0.00^{+1.6}_{-0.00}$
σ_J^2 ..	RV Jitter Variance	5^{+58}_{-41}	$0.1^{+2.7}_{-2.8}$	$-0.1^{+2.8}_{-2.7}$
K2-114				
Telescope Parameters:		HIRES		
$\gamma_{\rm rel}$.	Relative RV Offset (m/s)	$-40.8^{+6.7}_{-6.8}$		
σ_J ..	RV Jitter (m/s)	$11.9^{+3.8}_{-4.9}$		
σ_J^2 ..	RV Jitter Variance	141^{+100}_{-93}		
K2-115				
Telescope Parameters:		HIRES		
$\gamma_{\rm rel}$.	Relative RV Offset (m/s)	25^{+12}_{-13}		
σ_J ..	RV Jitter (m/s)	$26^{+21}_{-10.}$		
σ_J^2 ..	RV Jitter Variance	710^{+1600}_{-440}		
K2-180				
Telescope Parameters:		HARPS-N		
$\gamma_{\rm rel}$.	Relative RV Offset (m/s)	$-76614.40^{+0.58}_{-0.62}$		
σ_J ..	RV Jitter (m/s)	0.00		
σ_J^2 ..	RV Jitter Variance	$-3.6^{+3.2}_{-1.0}$		
K2-182				
Telescope Parameters:		HIRES		
$\gamma_{\rm rel}$.	Relative RV Offset[4] (m/s)	-1.8 ± 1.6		
σ_J ..	RV Jitter (m/s)	$4.6^{+1.9}_{-1.2}$		
σ_J^2 ..	RV Jitter Variance	$21.6^{+21}_{-9.8}$		

K2-237					
Telescope Parameters:		CORALIE	FIES	HARPS (Smith)	HARPS (Soto)
$\gamma_{\rm rel}$.	Relative RV Offset (m/s)	-22252 ± 40	-22507^{+15}_{-16}	$-22325.7^{+9.0}_{-9.4}$	-22252 ± 14
σ_J ..	RV Jitter (m/s)	110^{+49}_{-31}	$0.00^{+39}_{-0.00}$	18^{+22}_{-16}	$6.0^{+8.8}_{-6.0}$
σ_J^2 ..	RV Jitter Variance	12200^{+13000}_{-5800}	-70^{+1600}_{-520}	340^{+1300}_{-330}	40^{+180}_{-220}

K2-260				
Telescope Parameters:		FIES		
$\gamma_{\rm rel}$.	Relative RV Offset (m/s)	29072^{+22}_{-24}		
σ_J ..	RV Jitter (m/s)	$0.00^{+60}_{-0.00}$		
σ_J^2 ..	RV Jitter Variance	-600^{+4200}_{-2000}		
K2-261				
Telescope Parameters:		FIES	HARPS	HARPS-N
$\gamma_{\rm rel}$.	Relative RV Offset (m/s)	$-13.5^{+2.7}_{-2.8}$	$3340.2^{+2.3}_{-2.4}$	$3335.3^{+2.1}_{-2.6}$
σ_J ..	RV Jitter (m/s)	$4.6^{+4.0}_{-4.6}$	$6.6^{+2.7}_{-1.8}$	$5.6^{+4.2}_{-2.4}$
σ_J^2 ..	RV Jitter Variance	20^{+53}_{-25}	43^{+43}_{-20}	31^{+64}_{-21}
K2-265				
Telescope Parameters:		HARPS		
$\gamma_{\rm rel}$.	Relative RV Offset (m/s)	$-18185.56^{+0.52}_{-0.53}$		
σ_J ..	RV Jitter (m/s)	$5.71^{+0.43}_{-0.39}$		
σ_J^2 ..	RV Jitter Variance	$32.6^{+5.1}_{-4.3}$		

Notes. σ_J^2 was bound to ±300 m/s for K2-114 and the Soto et al. (2018) RVs for K2-237. For K2-98 σ_J^2 was bound to ±100 m/s for the FIES RVs and ±4 m/s for HARPS and HARPS-N. See §2.3 for discussion.